Characterization of offline analysis of particulate matter with FIGAERO-CIMS

Jing Cai[1,2,#], Kaspar R. Daellenbach[1,2,3,#,*], Cheng Wu[4,5], Yan Zheng[6], Feixue Zheng[1], Wei Du[1,2], Sophie L. Haslett[4], Qi Chen[6], Markku Kulmala[1,2], Claudia Mohr[4,*]

[1] Aerosol and Haze Laboratory, Beijing Advanced Innovation Center for Soft Matter Science and Engineering, Beijing University of Chemical Technology, Beijing 100029, China

[2] Institute for Atmospheric and Earth System Research, Faculty of Science, University of Helsinki, Helsinki 00014, Finland

[3] Laboratory of Atmospheric Chemistry, Paul Scherrer Institute, Villigen, Switzerland.

[4] Department of Environmental Science, Stockholm University, Stockholm, 11418, Sweden

[5] Department of Chemistry and Molecular Biology, Atmospheric Science, University of Gothenburg, Gothenburg, SE-412 96, Sweden

[6] State Key Joint Laboratory of Environmental Simulation and Pollution Control, Beijing Innovation Center for Engineering Science and Advanced Technology, College of Environmental Science and Engineering, Peking University, Beijing, 100871, China

[#] These authors contributed equally to this work.

Correspondence to: kaspar.dallenbach@helsinki.fi and claudia.mohr@aces.su.se

Abstract: Measurements of the molecular composition of organic aerosol (OA) constituents improve our understanding of sources, formation processes, and physicochemical properties of OA. One instrument providing such data at a time resolution of minutes to hours is the Chemical Ionization time-of-flight Mass Spectrometer with Filter Inlet for Gases and AEROsols (FIGAERO-CIMS). The technique collects particles on a filter, which are subsequently desorbed, and the evaporated molecules are ionized and analyzed in the mass spectrometer. However, long-term measurements using this technique and/or field deployments at several sites simultaneously, require substantial human and financial resources. The analysis of filter samples collected outside the instrument (offline) may provide a more cost-efficient alternative and makes this technology available for the large number of particle filter samples collected routinely at many different sites globally. Filter-based offline use of the FIGAERO-CIMS limits this method albeit to particle-phase analyses, likely at reduced time resolution compared to online deployments. Here we present the application and assessment of offline FIGAERO-CIMS, using Teflon and Quartz fiber filter samples that were collected in autumn 2018 in urban Beijing. We demonstrate the feasibility of the offline application with "sandwich" sample preparation for the identified over 900 organic compounds with (1) high signal-to-noise ratios, (2) high repeatability, and (3) linear signal response to the filter loadings. Comparable overall signals were observed between the Quartz fiber and Teflon filters for 12-h and 24-h samples, but with larger signals for semi-volatile compounds for the Quartz fiber filters, likely due to adsorption artifacts. We also compare desorption profile (thermogram) shapes for the two filter materials. Thermograms are used to derive volatility qualitatively based on the desorption temperature at which the maximum signal intensity of a compound is observed (T_{max}). While we find that T_{max} can be determined with high repeatability (±5.7°C) from the duplicate tests for one filter type, we observe considerable differences in T_{max} between the Quartz and Teflon filters, warranting further investigation into the thermal desorption characteristics of different filter types. Overall, this study provides a basis for expanding OA molecular characterization by FIGAERO-CIMS to situations where and when deployment of the instrument itself is not possible.

1. Introduction

Molecular information on organic aerosol (OA) composition is important for understanding the role that OA plays in the atmosphere regarding its impacts on air quality, human health, and the climate (Daellenbach et al., 2020; Huang et al., 2014; Cappa et al., 2012; Yao et al., 2018; Riipinen et al., 2012). Such data can be obtained from offline filter collection and analysis in the laboratory using optical (e.g. Fourier transform infrared spectroscopy, FTIR) and magnetic (e.g. Nuclear magnetic resonance spectroscopy, NMR) spectroscopy or, more commonly, high-resolution mass spectrometer methods, which include gas/liquid chromatography coupled to mass spectrometry (GC/LC-MS), ultrahigh-performance liquid chromatography coupled to Orbitrap mass spectrometry and electrospray ionization mass spectrometry (ESI-MS) (Noziere et al., 2015). In contrast, online mass spectrometers provide direct and in-situ information on particles' molecular composition, e.g. the filter inlet for gases and aerosols coupled to a high-resolution time-of-flight chemical ionization mass spectrometer (FIGAERO-HR-ToF-CIMS, Aerodyne Research Inc., US, hereafter FIGAERO-CIMS (Lopez-Hilfiker et al., 2014)), single particle mass spectrometer (Cai et al., 2015) or the extractive electrospray ionization time-of-flight mass spectrometer (EESI-MS) (Lopez-Hilfiker et al., 2019). Since the particle-phase measurement by FIGAERO-CIMS is filter-based, it has the potential to be used for offline analysis. Briefly, in the FIGAERO, particles are collected on a Teflon® (hereafter Teflon) filter and analyzed via thermal desorption. When coupled to a high-resolution time-of-flight chemical-ionization mass spectrometer (hereafter CIMS), molecular composition information of inorganic and organic aerosol compounds that evaporate at temperatures up to 200 °C can be achieved. Having the advantage of combining molecular composition and volatility information, the FIGAERO-CIMS has been widely used for measuring OA compounds in many different environments including e.g. forests (Lopez-Hilfiker et al., 2016; Lee et al., 2016; Lee et al., 2018; Mohr et al., 2019), rural and urban areas (Le Breton et al., 2019; Huang et al., 2019a; Cai et al., 2022), indoor air (Farmer et al., 2019), and cooking emissions (Masoud et al., 2022).

Both online and offline techniques have their advantages and disadvantages and are associated with artefacts (Turpin and Lim, 2001; Turpin et al., 2000). Both online and offline techniques have their advantages and disadvantages and are associated with artefacts (Turpin and Lim, 2001; Turpin et al., 2000). Offline techniques are an easy alternative to demanding online in-situ approaches requiring large human and financial resources. Moreover, one collected filter can be used for different analysis methods and purposes. However, the offline approaches are susceptible to sample handling and storage artefacts. The condensation and re-evaporation of vapors, and potential reactions on the filter during sampling and storage can result in both positive and negative sampling biases (Turpin et al., 2000; Cheng et al., 2009). Online instruments generally allow for measurements at higher time resolution, which is an advantage when studying rapid atmospheric processes, and no sample storage is needed before analysis. However, the deployment of the FIGAERO-CIMS outside the laboratory requires a well-equipped site that is easily accessible. In addition, long-term maintenance of these complex mass spectrometers needs substantial human and financial resources. Therefore, deployments are often achieved only for short periods (i.e. campaigns lasting from a couple of weeks to months), which limits the application of this technique for monitoring and simultaneous measurements at multiple sites. Furthermore, FIGAERO gas-phase measurements have to be interrupted regularly for particle-phase analysis in online usage, which could be a problem for measurements requiring high time resolution data (e.g. chamber studies). Using the FIGAERO-CIMS for analyzing filters collected elsewhere ("offline application") may therefore provide a valid alternative for long-term monitoring or simultaneous measurements at multiple sites. Whereas the online FIGAERO-CIMS technique typically uses Teflon filters to reduce interferences from the gas phase, Quartz fiber filters are widely used for offline sampling of OA due to their high melting point and insolubility in water and typical organic solvents (Watson and Chow, 2002; Tao et al., 2017; Schauer et al., 2002; Gustafson and Dickhut, 1997). Up to now, only a few studies have used the FIGAERO-CIMS in offline mode with Teflon filters (Siegel et al., 2020; Huang et al., 2019b), and an in-depth characterization of the method is missing. The performance of Quartz fiber filters in FIGAERO-CIMS needs to be assessed and compared to Teflon filters.

Here, we describe the application of FIGAERO-CIMS in offline mode for the analysis of particles deposited on Teflon and Quartz fiber filters in urban Beijing during the autumn and winter of 2018. The filter deposition time

varies from 30 min to 24 h. We assess the performance of FIGAERO-CIMS for offline characterization of OA as well as inorganic compounds and discuss background determination, reproducibility, and linearity of response for the two filter types. We describe filter handling and offline analysis procedures and show the comparison of signals from different mass loadings collected on both filter types. The utility of the FIGAERO for offline use is demonstrated in this study. The potential to broaden its application for OA component measurements in future research is also discussed. We note, however, that it is not the scope of this paper to discuss aspects of offline FIGAERO-CIMS that also apply to its online deployment, such as e.g. general percentage of recovery from the filter or calibrations.

2. Methods

2.1 Filter sampling

The sampling site is situated on the west campus of the Beijing University of Chemical Technology (BUCT, 39° 56'31" N, 116°17'50" E). BUCT is located near the West Third Ring Road of Beijing, surrounded by residential areas. A more detailed description of the sampling site can be found elsewhere (Cai et al., 2020; Kontkanen et al., 2020; Liu et al., 2020; Yao et al., 2020; Fan et al., 2021; Guo et al., 2021). From November to December 2018, samples of fine particulate matter with an aerodynamic diameter of up to 2.5 μm ($PM_{2.5}$) were collected by a four-channel sampler (TH-16A, Tianhong Co., China) with a sampling flow rate of 16.7 L min^{-1}, installed on the rooftop of a five-floor building (~20m above ground). Both Teflon (Zefluor® PTFE membrane, 1 μm pore size, 47 mm diameter, Pall Corp., US) and Quartz fiber filters (7202, 47 mm diameter, Pall Corp., US) were collected simultaneously at separate channels. The four parallel channels of the sampler had a shared PM_{10} cyclone inlet and were equipped with 4 independent $PM_{2.5}$ cyclones and auto flow controllers for each channel. All channels were measuring the same size range of particles. A sizing effect from the interactions between different channels can therefore be neglected. The setup of filter type for each channel was as follows: Channel 1, Teflon (12 h for or 0.5 h); Channel 2, Quartz (12 h or 0.5 h); Channel 3, Teflon (24 h or 2.5 h); Channel 4, Quartz filters (24 h or 2.5 h). This is listed in Table 1. The flow rate was regularly calibrated individually for each channel during the sampling process.

To investigate the influence of filter mass loadings and collection time on the signal response, the following filter samples were taken: (1) 5 pairs of samples (Teflon/Quartz fiber filters, Channels 1 and 2) with 30 min deposition time on Dec 15, 2018 between 14:00 to 16:30 (Table 1). At the same time, an additional pair of Teflon/Quartz samples were deposited for 2.5 hours using the other two separate channels of the sampler (Channels 3 and 4). (2) 12-h samples of Quartz/Teflon filters (Channels 1 and 2) from Oct 26 to Oct 30 and Nov 3 to Nov 24 (here only the Quartz filters from Nov 3 to Nov 16 were analyzed (in total 27 pairs of samples), shown in Table 1). (3) 24-h Quartz/Teflon samples (Channels 3 and 4) from Oct 26 to Oct 30 and Nov 3 to Nov 25 (here only one pair of Teflon/Quartz filters was analyzed, shown in Table 1). During the last sampling period, high $PM_{2.5}$ and relative humidity (RH) conditions prevailed (Nov 3:181 μg m^{-3}, 60%, and Nov 13: 227 μg m^{-3}, 75%), and the channel of the 24-h sampling Teflon filter got clogged. Thus, only one pair of 24-h Teflon/Quartz samples from this period was analyzed (Table 1).

Detailed information on the sampling protocol is listed in Table 1. Three pairs (Teflon/Quartz) of field blank samples were also collected during the sampling period. Before sampling, Teflon filters were baked for 2 hours at 200 °C, which is much longer than the typical desorption time for FIGAERO-CIMS online usage (Ylisirniö et al., 2021), and Quartz filters for 4.5 hours at 550 °C (Liu et al., 2016) in order to minimize contamination. After sampling, samples were put in filter holders wrapped in pre-baked aluminum foils, individually sealed in a sealed bag and stored in a freezer at -20 °C for 7 months until being analyzed in the laboratory.

To calculate the OA mass loadings of the samples, an online Time-of-Flight-Aerosol Chemical Speciation Monitor (Aerodyne Research Inc., US, hereafter ToF-ACSM) equipped with a $PM_{2.5}$ lens and standard vaporizer

was operated during the sampling period at the same site. Details of the ToF-ACSM settings can be found in Cai et al. (2022). The OA loading on each filter (OA_{filter}) was determined relying on the OA concentrations from the co-located TOF-ACSM (OA_{ACSM}), the offline filter sampling flow rate (16.7 L min^{-1}), the sampling time, the surface of the entire offline filter sample (A_{filter}), and the analyzed offline filter sample (A_{punch}) (Equation 1):

$$OA_{filter} = \frac{A_{punch}}{A_{filter}} \times OA_{ACSM} \times Sampling\ flow\ rate \times Sampling\ time \quad (1)$$

Table 1: Testing objectives, filter deposition dates and times, flows, filter material (T = Teflon, Q = Quartz fiber), filter mass loadings of OA, number of samples, and number of sample repeats (filter punches) for the same filter.

Testing objective	Sampling date	Sampling time	Filter material	OA loading [µg] per punch (punch diameter, area)	Number of samples/repeats
(1) Baseline subtraction tests, (2) reproducibility tests, (3) filter type comparison	Dec 15 14:00 – 16:30 (30 min-interval)	30 min	T & Q	1.7×10^{-2}–2.0×10^{-2} (2 mm, 0.031 cm^2)	1/1
	Dec 15, 14:00 – 16:30	2.5 h	T & Q	9.1×10^{-2} (2 mm, 0.031 cm^2)	1/3 for repeats
(1) Reheating tests, (2) filter type comparison	Nov 8 21:30– Nov 9 9:00	12 h	T & Q	6.5×10^{-1} (2 mm, 0.031 cm^2)	1/1
Reheating tests	Nov 12 21:30– Nov 13 9:00	12 h	Q	0.75 (2 mm, 0.031 cm^2)	1/1
Reheating tests	Nov 13 21:30– Nov 14 9:00	12 h	Q	1.2 (2 mm, 0.031 cm^2)	1/1
(1) Filter type comparison, (2) different ramping protocols for 2 mm punch, (3) linearity response for signals from different filter punch areas	Nov 24 9:30– 9:00 25	24 h	T & Q	1.2 (2 mm, 0.031 cm^2)	1/3 for repeats and 1/3 for different ramping protocols
				2.7 (3 mm, 0.071 cm^2)	1/1
				4.8	1/1

				(4 mm, 0.13 cm^2)	
				15 (7 mm, 0.38 cm^2)	1/1
Comparison of 12-h signals to ToF-ACSM	Nov 3 to Nov 16	12 h	Q	5.0×10^{-2} – 1.2 (2 mm, 0.031 cm^2)	27/1

141

142

143 **2.2 Offline application of FIGAERO-CIMS**

144 **2.2.1 Measurement approach**

145 **2.2.1.1 FIGAERO-CIMS setup**

146 The molecular composition of OA collected on the filter samples was characterized with FIGAERO-CIMS using
147 iodide (I^-) as the reagent ion. In typical online FIGAERO-CIMS operation, particles are collected on a filter
148 (Zefluor® Teflon filters) with a sampling time of a few minutes to hours and then thermally desorbed by a flow of
149 temperature-controlled ultra-pure nitrogen (99.999 %) immediately following deposition. The thermally desorbed
150 compounds are charged by clustering with I^-, which is typically generated through the exposure of methyl iodide
151 to an X-ray or radioactive source for FIGAERO-CIMS (Po^{210} in our study). In this study, we used the FIGAERO-
152 CIMS in the laboratory to analyze filter samples collected earlier in the field. These samples were placed manually
153 one by one in the dedicated filter holder of the FIGAERO-CIMS and the desorption procedure was started (see
154 2.2.1.3).

155 **2.2.1.2 Sample preparation and test design**

156 Since the total particle mass collected on one filter was generally too large to be analyzed at once in its entirety
157 by FIGAERO-CIMS (due to the risk of titration of the reagent ion), we only analyzed small circular punches of
158 the collected filters. The default punching area was 3.1×10^{-2} cm^2 (punch diameter d=2 mm). In addition, to test the
159 linearity of response to sample mass loadings, punch areas for the same filter were varied between 3.1×10^{-2} cm^2
160 (d=2 mm) and 0.38 cm^2 (d=7mm), resulting in variation in mass loadings by a factor of 10 (shown in Table 1).
161 Since the filter punches were too small for the filter holder of the FIGAERO, we put them between two pre-baked
162 originally sized (d=25 mm) Zefluor® Teflon filters ("sandwich technique", Fig. 1a). Field blanks were prepared
163 analogously.

164 The OA mass loadings of the filter punches were estimated with the co-located ToF-ACSM in this study (details
165 shown in Table 1). To test the performance of the method, we did the following tests (Fig. 1, Table 1): (1) reheating
166 a few filters to determine backgrounds (see section 2.2.4), (2) assess different background subtraction methods,
167 (3) reproducibility of signals from the same filter (section 3.4), (4) the linearity of signal response from different
168 punching areas from the same filter (section 3.4), (5) comparing signals from different ramping protocols (section
169 2.2.1.3), (6) comparison between and offline FIGAERO-CIMS and online ToF-ACSM (section 3.5), (7) signals
170 from different filter types (section 3.6), and (8) thermograms from different types of filters (section 3.7).

2.2.1.3 Temperature ramping protocols

Reagent ion depletion is undesired as it can create non-linearities in the instrument response (Koss et al., 2018; Zheng et al., 2021). To avoid reagent ion depletion in FIGAERO-CIMS, the concentration of sample ions entering the instrument is controlled, typically by modifying the particle mass loading on the filter and/or the heating rate. While the particle mass loading can be varied easily when operating the FIGAERO-CIMS online through adjustment of sampling time and flow, in offline mode with pre-collected samples this can only be modified by the fraction of filter surface analyzed. For our Beijing filter samples, even when using the smallest punch sizes (3.1×10^{-2} cm^2), mass loadings of especially nitric acid (HNO_3) were still high enough to lead to titration of the reagent ion. We note that this can also be an issue for online measurements in presence of high nitrate concentrations, e.g. in highly polluted areas. In order to reduce reagent ion depletion between 60 °C to 105 °C desorption temperature, where HNO_3 exhibits a maximum signal, we used a heating protocol with a non-uniform temperature ramping procedure. Instead of ramping from room temperature to 200 °C with a constant heating rate, we divided the temperature ramp into several periods: (1) from room temperature (~25 °C) to 60 °C in 8 min (4.4 °C min^{-1}), (2) from 60 °C to 105 °C in 15 min (3 °C min^{-1}), (3) from 105 °C to 200 °C in 12 min (7.9 °C min^{-1}). The ramp period was followed by a 20-minute soaking period (200 °C) to allow signals to go to background levels. We called this temperature ramping protocol non-uniform temperature ramping and used it as the default desorption procedure in this study. The maximum reagent ion depletion achieved in this way was ~35% for the samples with the highest mass loadings on a 2 mm punch, which was mostly used in this study. We also tested two alternative heating protocols:

1) Slow non-uniform temperature ramping: Same as the non-uniform ramping protocol, but with (2) slowed down to 1.5 °C min^{-1}. The total heating time for this protocol was 70 minutes, and the maximum reagent ion depletion was ~ 20%.
2) Uniform temperature ramping: The temperature was increased from room temperature to 200 °C in 31.5 min (5.7 °C min^{-1}). Including the 20 min soak, the total heating was 51.5 minutes, and the maximum reagent ion depletion was around 50%. In order to limit reagent ion depletion, the heating rate was 1.8–3.5 times slower than typical rates used for online FIGAERO-CIMS applications (10–20 °C min^{-1} (Thornton et al., 2020)).

The 3 temperature ramping protocols are displayed in Fig. 1d. As different heating rates lead to different thermogram shapes and T_{max} for individual compounds, we developed a correction method in an effort to be able to compare desorption-derived volatility for the different ramping protocols. This will be further discussed in section 3.3.

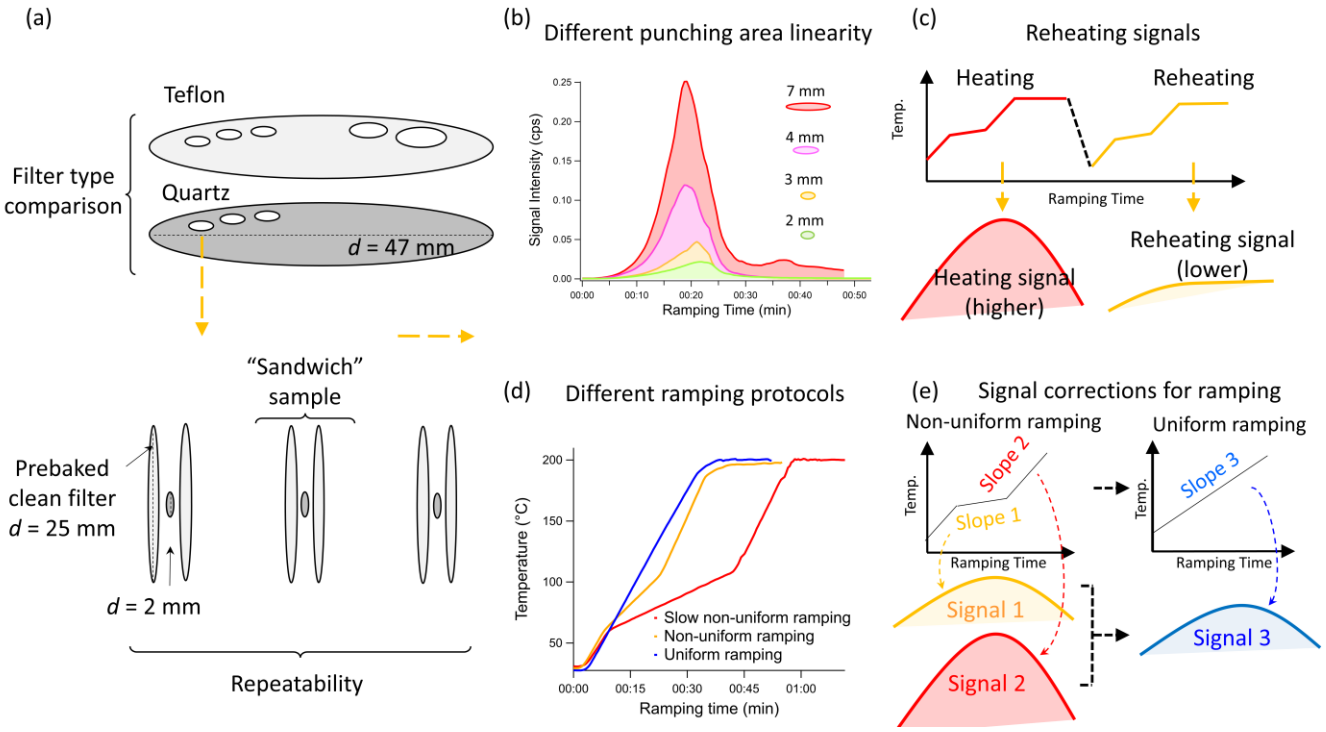

Figure 1. Schematic of the tests conducted in this study, (a) sample preparation using punching areas of different sizes of the Teflon and Quartz fiber filters and squeezing them between two original-sized filters for analysis, (b) signal intensities of different punching areas from the same sample with the same analytical procedure, (c) reheating tests by conducting two consecutive heating cycles, (d) different temperature procedures, and (e) signal intensity correction from non-uniform ramping to uniform ramping.

2.2.2 Data analysis

In this study, FIGAERO-CIMS data were analyzed with the Tofware package (v.3.1.0, Tofwerk, Switzerland, and Aerodyne, US) within the Igor Pro software (v.7.08, Wavemetrics, US). Mass accuracies of low- to high-mass species (~130 to 500 Da) were within ±10 ppm for all the samples. A total of ~1,200 peaks were found in the range of 46 and 500 Da, of which 916 were identified as organic species. Detailed information about the identified chemical compounds can be found in Cai et al. (2022). The total signal of a compound per filter sample, defined as the integrated signals (*Is*), calculated by first normalizing by the signals of the primary ions (I^-) and then integrating the entire thermogram (ramping and soaking, normalized by the signals of I^-). Signals of the first 1.5 min of ramping and the last 1.5 min of soaking periods were excluded in order to remove potential interference from switching to and from the heating status. In this study, we use the term CHOX to represent all organic compounds identified by FIGAERO-CIMS, $C_{x\geq1}H_{y\geq1}O_{z\geq1}X_{0-n}$, detected as clustered with I^-, with X being different atoms including N, S, Cl, or a combination of them.

2.2.3 Background subtraction

The background in offline FIGAERO-CIMS is a combination of instrument background and field blank. The field blanks provide information on sampling and handling artefacts, while the instrument background is mainly from (1) the desorption of semi-volatile or low-volatile compounds adsorbed on instrument surfaces (such as the ion-molecular reaction region (IMR)), and (2) impurity of the reagent ion precursors and carrier gases. Thus, instrument background signal can vary for different samples and depending on instrument status. For FIGAERO-CIMS online deployments, frequent blank measurements and calibrations are recommended (Bannan et al., 2018;

Thornton et al., 2020). The common method for online FIGAERO-CIMS of placing an additional filter upstream of the FIGAERO filter is impossible for offline pre-sampled filters. Given *1)* the large variation of the filter sample loadings (~1×10^{-2} µg – 1.2 µg), which influences the number of compounds that can potentially adsorb to instrument surfaces, *2)* the general scarcity of field blanks in offline mode compared to background filter samples in online FIGAERO-CIMS, and *3)* that the instrument background can be influenced by instrument history very different from the offline sample due to the temporal separation of sample and analysis, choosing an appropriate instrumental and field blank determination method is crucial and challenging for offline FIGAERO-CIMS analysis. Here we describe and discuss performance of 6 different background subtraction methods (schematically shown in Fig. 2):

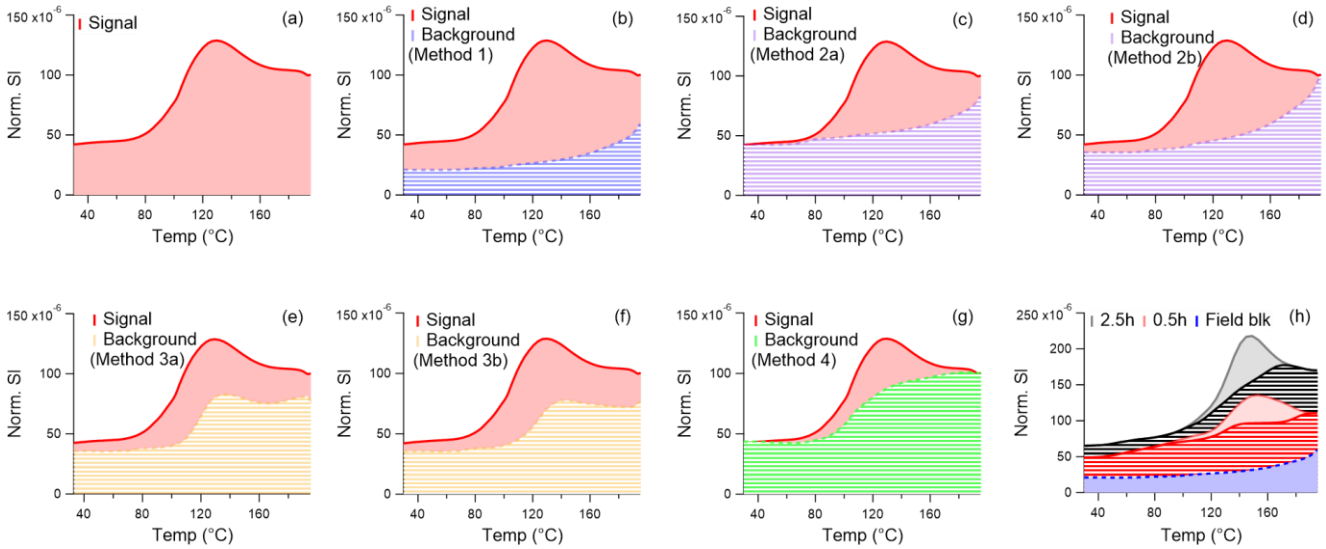

Figure 2. Schematic of a compound's signal and background thermograms for different background determination methods. The x-axis is the temperature during ramping, and the y-axis is the signal intensity normalized by the primary ion (I^-). (a) total sample signal of a model compound without blank subtraction, (b) Method 1: field blank only, (c) Method 2a: scaling field blank to the start of ramping, (d) Method 2b: scaling field blank to the end of soaking, (e) Method 3a: reheating of a subset of filters, and using the average signal ratio from reheated and heated filters as background signal for all filters (individual compound-based), (f) Method 3b: reheating of a subset of filters, and using an exponential fit to the entire mass range of the average signal ratio from reheated and heated filters as background signal for all filters, (g) Method 4: thermal baseline using a spline algorithm, and (h) one 0.5-h and one 2.5-h sample with blank-subtraction. Ideally, the *Is* of the 2.5-hour collection sample ($Is_{2.5h}$) would be close to the sum of the 5 paralleled 0.5-hour collection sample ($Is_{0.5h}$).

Method 1: Background is the average integrated signal intensity (*Is*, the integrated signal of the thermograms shown in Fig. 2a) of field blanks ($\overline{Is_{field\ blk,i}}$), which are three in our case (Fig. 2b). The integrated background-subtracted signal for compound *i* ($Is_{blksub,i}$) is then $Is_i - \overline{Is_{field\ blk,i}}$.

Method 2: Background is field blank average ($\overline{Is_{field\ blk,i}}$, see Method 1) scaled to the ratio of ambient sample and field blank signals during a reference period (ref period) – either prior to the start of heating (the first 1.5 to 3 min of the ramping procedure before the temperature starts to increase, Method 2a or at the end of the soaking (the last 1.5 to 3 min of the soaking period, Method 2b). Method 2 corrects for variation in instrument background that is not necessarily related to the sample to be analyzed. The integrated background-subtracted signal for compound *i* ($Is_{blksub,i}$) is then

$$Is_{blksub,i} = \int I_{sample,ij} - \int I_{field\ blk,ij} \times \frac{\int^{ref\ period} Is_{i,ambient}}{\int^{ref\ period} Is_{i,field\ blk}} \qquad (2)$$

By using Method 2a, it is assumed that the signal measured before heating, but with the filter already in place, is due to instrument background, which can vary between the measurement of a sample filter and a blank filter (Fig. 2c). However, this method may lead to underestimation of the sample signal for compounds that already evaporate at room temperature.

By using Method 2b, it is assumed that the signal measured at the end of soaking is due to instrument background, which can vary between the measurement of a sample filter and a blank filter. The variation in instrument background is taken into account at maximum heating temperature (200 °C) and thus elevated temperature of surfaces downstream of the filter, and at the end of the soaking period when presumably all material that can evaporate from the filter has evaporated (shown in Fig. S1).

Method 3: In this method (Siegel et al., 2021), the instrument background is assessed by heating the same filter twice, assuming that during the first heating cycle, all detectable material has evaporated, and that what is measured in a reheating cycle is the instrument background signal. Ideally, reheating would be done for each sample individually. Since this was not done for our dataset, the instrument background determined based on a few reheats (3 in our case, the details of the reheating samples are shown in Table 1) had to be extrapolated to all samples (Method 3a and 3b). It is clearly shown that the signals from the reheating cycle are much lower than those from the first heating (Fig. S1) without a clear peak in thermograms for both filter types, suggesting sampled compounds were well desorbed in the original heating cycle. Simple reheating does not consider the field blanks, which need to be subtracted in addition.

For Method 3a we assumed that the ratio of the integrated signal of the second heating cycle (heating C2) and first heating cycle (heating C1) of the same filter is influenced by volatility and therefore compound-dependent. Here we used the average ratio from 3 reheating tests done for this dataset (Fig. S2). The distribution of the ratios is shown in Fig. S3. The $Is_{blksub,i}$ was then calculated following Eq. 2, where the instrument background is the fraction of the sample signal established from the re-heating, and added to the signal from the field blank, which is calculated in the same way.

$$Is_{blksub,i} = \left(Is_{sample,i} - Is_{sample,i} \times Is_{i,\left(\frac{heating\ C2,i}{heating\ C1,i}\right)} \right) - \left(Is_{field\ blk,i} - Is_{field\ blk,i} \times Is_{i,\left(\frac{heating\ C2,i}{heating\ C1,i}\right)} \right) \quad (3)$$

For Method 3b, we assumed that the ratio of heating C2 to heating C1 exhibits a signal dependency (relatively higher background for compounds with lower signal), calculated using an exponential fit to the data from the 3 reheat tests (Fig. S4) using Eq. (4) with the constants A, B, and C. The field blanks are calculated in the same way. Then the Is_{blksub} can be calculated as in Eq. (3)

$$Is_{i,\left(\frac{heating\ C2,i}{heating\ C1,i}\right)} = A + B \times \exp\left(Is_{sample,i} + \mathrm{C}\right) \quad (4)$$

Method 4: Thermal baseline subtraction. In this method, we determined for every thermogram of each compound a background thermogram termed thermal baseline (Is_{thbsl}). The thermal baseline was computed using a spline algorithm initially developed by Wang et al. (2018) for determining the background concentration of a pollutant using its concentration time series (by determining the spline of background from varying time intervals). Thermogram data were pre-averaged to 1.8 mins (corresponding to 4 data points of the original time resolution of 27s) to reduce noise for the thermal baseline computation. Field blanks were handled in the same way (shown in Fig. S5). Thus, the blank-subtracted signal Is_{blksub} of a compound *i* is:

$$Is_{blksub,i} = Is_{sample,blksub,i} - Is_{field\ blk,blksub,i} = \left(\int I_{sample,i,j} - Is_{sample,thbsl,i} \right) - \left(\int I_{field\ blk,i,j} - Is_{field\ blk,thbsl,i} \right) \quad (5)$$

298 $Is_{sample,\ thsbl,i}$ and $Is_{field\ blk,\ thbsl,I}$ represent the thermal baseline of compound *i* for samples and field blanks, respectively.

299 **2.2.4 Thermograms and T_{max} recovery**

300 The amount of compounds coming off the filter at a certain temperature varies as a function of temperature
301 ramping rates, resulting in different thermogram shapes and T_{max} (shown in Fig. 1d). This is especially important
302 in our case for the non-uniform ramping protocols. In an attempt to make the different cases comparable for
303 qualitative volatility studies, we developed a thermogram correction where the blank-subtracted signal as a
304 function of temperature for each compound *i* is re-distributed to constant temperature intervals (Eq. (6)):

305 $$I_{thermocorrected,i,j} = \int_{T-\Delta t}^{T} I_{sample,blksub,i,j}\, dT \qquad (6)$$

306 Considering the ~2 °C variation in thermogram reproducibility reported from an online FIGAERO-CIMS study
307 (Lopez-Hilfiker et al., 2014), the temperature interval ΔT used in this study is 3°C.

308

309 **3. Results**

310 **3.1 Assessment of the background: Signal comparison between different blank subtraction methods**
311 To assess the influence of the 6 background methods on the resulting signal, Quartz fiber filter samples from 5
312 different 0.5-h samples (OA: ~2.0×10^{-2} μg for each punch) and a 2.5 h sample collected in parallel (OA: 9.1×10^{-2}
313 μg) were used, and the sum of their background-subtracted integrated signals (Is_{blksub}) compared (Fig.2 h). Without
314 background subtraction, the sum of the signals from the five 0.5-h samples was generally higher than the *Is* of the
315 2.5-h sample (shown in Fig. 3a). An exception to this is HNO_3^-, which has the highest signal of all compounds and
316 therefore is the least influenced by background. The higher *Is* for the sum of the five 0.5-h samples is likely because
317 of the low signal-to-noise ratio compared to the 2.5-h sample. Subtracting only the field blank (Method 1) therefore
318 yielded the same result (Fig. 3b). Scaling the heating baseline (Method 2a and 2b) led to a better agreement between
319 the sum of the five 0.5-h and the 2.5-h samples (Figs. 3c and d). Compounds with high abundance generally fall
320 on a 1:1 line (slope range 0.5–2) by using these two background subtraction methods. With the thermal baseline
321 subtraction method (Method 4), results were comparable between 2.5-h and five 0.5-h samples. For the approach
322 using filter reheating (Method 3), there was a lesser agreement between the sum of the 0.5-h samples and the 2.5-
323 h sample (Figs. 3e and 3f). We speculate that this could be improved with a reheating cycle for every sample. For
324 future offline FIGAERO-CIMS analyses, we recommend carefully determining the background. Following our
325 assessment of blank determination methods, we suggest regular collections of field blanks and scaling their signal
326 (Methods 2a/b), and if field blanks are not available, computing a thermal baseline (Method 4). If using the
327 reheating approach as in a previous study with FIGAERO-CIMS in offline mode (Siegel et al., 2021), the
328 background should be determined by conducting reheating desorption cycles for each sample and blank
329 individually.

330 In general, as expected, high mass loadings are less sensitive to the various background subtraction methods due
331 to the higher signal-to-noise ratio (for example, 12-h/24-h sampling with OA loading of ~1 μg, Fig. S6). Besides
332 filter loadings, baseline levels can also be influenced by the properties of compounds (e.g. stickiness) and
333 instrument geometry. In summary, of all background subtraction methods shown here, Methods 2a, 2b, and 4
334 achieved the best agreement in signal intensities between the sum of 0.5-h and 2.5-h samples (Fig. S7). With these
335 methods, 82% to 93% of high-signal compounds (25% highest signal) fell into a signal ratio of ~1 (0–2, Fig. S8).
336 This shows the importance of correctly assessing the instrument background, especially for compounds with low
337 signal.

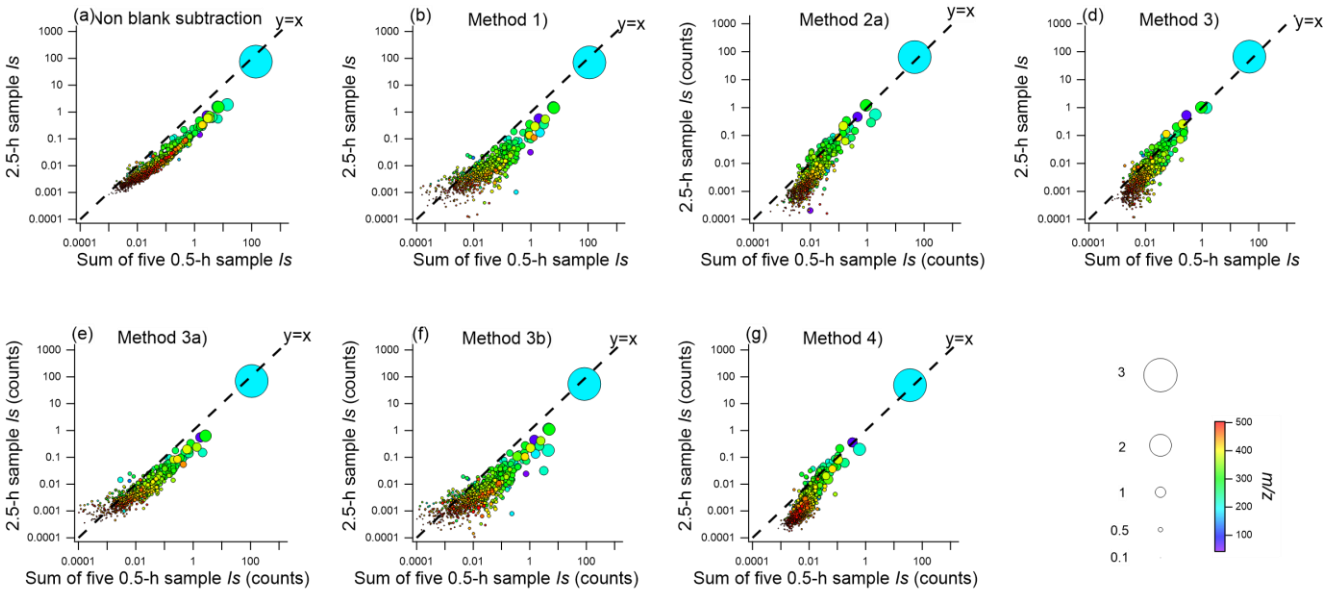

Figure 3. Comparison of the integrated signals (*Is*) for the 2.5-h versus sum of 0.5-h samples (a) without blank subtraction, with blank subtraction using (b) Method 1, (c) Method 2a, (d) Method 2b, (e) Method 3a, (f) Method 3b, (g) Method 4. The size of dots is proportional to the 4th root of integrated signal intensities of compounds, and they are color-coded by the ions' *m/z* (mass-to-charge ratio).

In this study, we applied Method 2b in the following discussions due to its better performance for the compounds with both higher (*Is*>0.1 counts) and lower signal (*Is*<0.01 counts, Fig. 3d). First, we examined the signal-to-noise ratios for offline FIGAERO-CIMS, defined as the ratio of the blank-subtracted signal to the standard deviation (STDs) of the background determined using method 2b per compound. Most of the identified compounds are above the estimated detection limit (3 times STDs of the backgrounds) for both filter types (87% and 87% of CHOX peaks for both 24-h Quartz and Teflon filters, OA loadings of 1.2 μg/3.1×10^{-2} cm^2 (2 mm punch)). For the 12-h samples (OA loadings of 0.58 μg/3.1×10^{-2} cm^2 (2 mm punch)), 84% and 70% of CHOX compounds were above the detection limit for Quartz and Teflon filters, respectively (Fig. S9). This varies for different filter loadings and punch areas.

3.2 Reproducibility of signal

We performed reproducibility tests using three 2-mm punches from the same 24-h and 2.5-h samples of both Teflon and Quartz filters and checked the signal response with the non-uniform temperature ramping procedure. The comparisons of the blank-subtracted CHOX *Is* for the 24-h and 2.5-h sample punches for both filter types are displayed in Fig. 4 and Fig. S10, respectively.

In Figs. 4a and 4b, we plotted the compounds' signal from one punch versus their average signal from all 3 punches for the Teflon and Quartz filters, respectively. We observe a high correlation between the individual and average signals (Spearman correlation coefficients Rsp are 0.95–0.96 and 0.97–0.99 for Teflon and Quartz filters, respectively). For each CHOX compound, we also computed the relative error (standard deviation/average signals (Std(*Is*)/Avg(*Is*) for the three punches) versus the average signal (Figs. 4c, 4d). The relative error for a CHOX compound was 9% for Quartz and 18% for Teflon (median relative errors) for 24-h samples (Figs. 4c, 4d). The relative error decreased with higher signal intensities (Figs. 4c, 4d), especially for the Quartz filters, suggesting that abundant compounds are measured more precisely than less abundant compounds. This trend is less apparent for Teflon filters, which is likely caused by less reproducibility for high *Is* compounds. Possible explanations could be uneven distribution of particulate mass on the filter or larger uncertainties in the punching process for Teflon filters due to the extension of the material. 86% and 94% of all CHOX compounds for Teflon and Quartz filters, respectively, had >3 times higher signals than the variability from the duplicate tests (Fig. S9). For the 2.5-h filter

samples (Fig. S10), the relative error is higher compared to the 24-h samples (25% for Quartz, and 31% for Teflon). This is likely due to the lower OA loadings (9.1×10^{-2} μg/punch) of the 2.5-h sample compared to the 24-h sample (1.2 μg/punch), which leads to higher uncertainties for blank subtraction and peak fitting. Still, the analytical reproducibility is acceptable, even for samples with OA loadings as low as ~0.1 μg. The relative error between repeats reported here is slightly larger (~9% and 18% for ~1 μg OA/punch for Quartz and Teflon filters, and 25% for Quartz, 31% for Teflon for ~0.1 μg OA/punch) compared to the variability in signal for online FIGAERO-CIMS (5–10% for 1 μg OA, (Lopez-Hilfiker et al., 2014)).

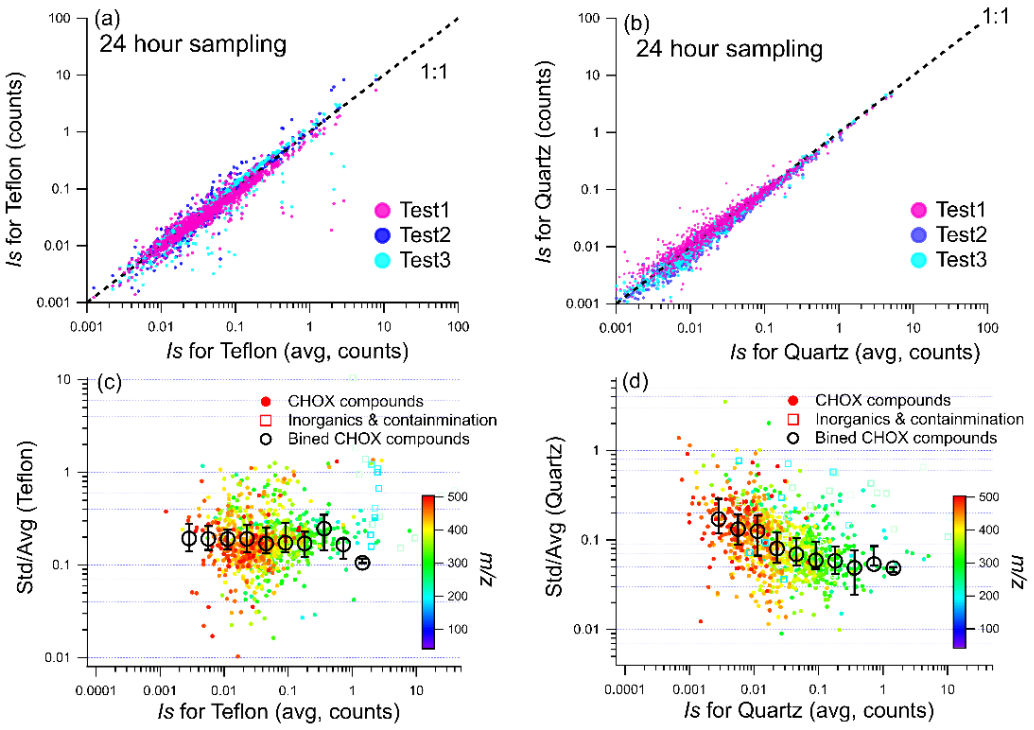

Figure 4. Comparison of the integrated signals from duplicate tests of the same 24-h sample for (a) Teflon and (b) Quartz fiber filters. The relative error (*Is* ratio of standard deviation/average) value of the 3 duplicate tests as a function of *Is* for (d) Teflon and (d) Quartz filters. In (c) and (d), CHOX compounds are shown as dots, inorganics as well as contaminants as squares colored by the *m/z*. The black circles in (c) and (d) represent median values of signal intensity bins (with log *Is* intervals of 0.3 for the *Is* range of 0 to 2) and error bars represent the 25th and 75th percentile of binned values of Std(*Is*)/Avg(*Is*) for CHOX.

3.3 Comparison of signal for different temperature ramping protocols

Here we compare the signal from different ramping protocols for the punches from the same 24-h Quartz and Teflon filters (Table 1). Since as suggested in the section 2.2.2, the *Is* were calculated by the integration of the normalized signals (normalized to the primary ion (I^-)), which to some extent compensates for reagent ion depletion. The signal of the field blanks is largely dominated by instrument background (i.e. there is no distinct peak in the thermogram (Fig. S1e) thus the *Is* of the field blanks is highly influenced by integration time. Since the field blanks were only analyzed with non-uniform ramping, the *Is* for slow non-uniform and uniform ramping protocols were assumed as the *Is* of non-uniform scaled by their integration time ratios.

The comparison of the background-subtracted *Is* of all identified compounds from different ramping protocols for a pair of 24-h Quartz and Teflon filters each is shown in Fig. 5. Since the integrated signals of the compounds within a mass spectrum are log-normally distributed (shown in Fig. S11a and S11b), a linear fit would be strongly biased by high-signal compounds such as HNO_3I^- or $C_6H_{10}O_5I^-$. Thus, we calculated the correlation coefficients of

the log-transformed signal intensities in the comparison. The Pearson correlation coefficients (Rp) and Spearman correlation coefficients (Rsp) are as follows: for Quartz filters Rp = 0.91, Rsp = 0.94 for non-uniform *vs* uniform, and Rp = 0.91, Rsp = 0.94 for slow non-uniform *vs* uniform, and for Teflon filters Rp = 0.82, Rsp = 0.78 for non-uniform *vs* uniform, and Rp = 0.83, Rsp = 0.70 for slow non-uniform *vs* uniform protocols.

These numbers suggest that the Quartz samples were less affected by different temperature ramping protocols than the Teflon samples. We also note that Teflon samples exhibited lower reproducibility than Quartz samples (see section 3.2). The lowest Rp and Rsp were observed for the comparison between the slow non-uniform ramping and the uniform ramping procedure for Teflon filters (Fig. 5d). Possible explanations could be the higher background and thus lower signal-to-noise ratios for Teflon filters in the low ramping rate region (1.3 °C min^{-1} for the range of 60 °C to 105 °C) of the slow non-uniform ramping protocol. Thus, care needs to be taken when using very slow heating rates and backgrounds need to be carefully assessed, especially for Teflon filters.

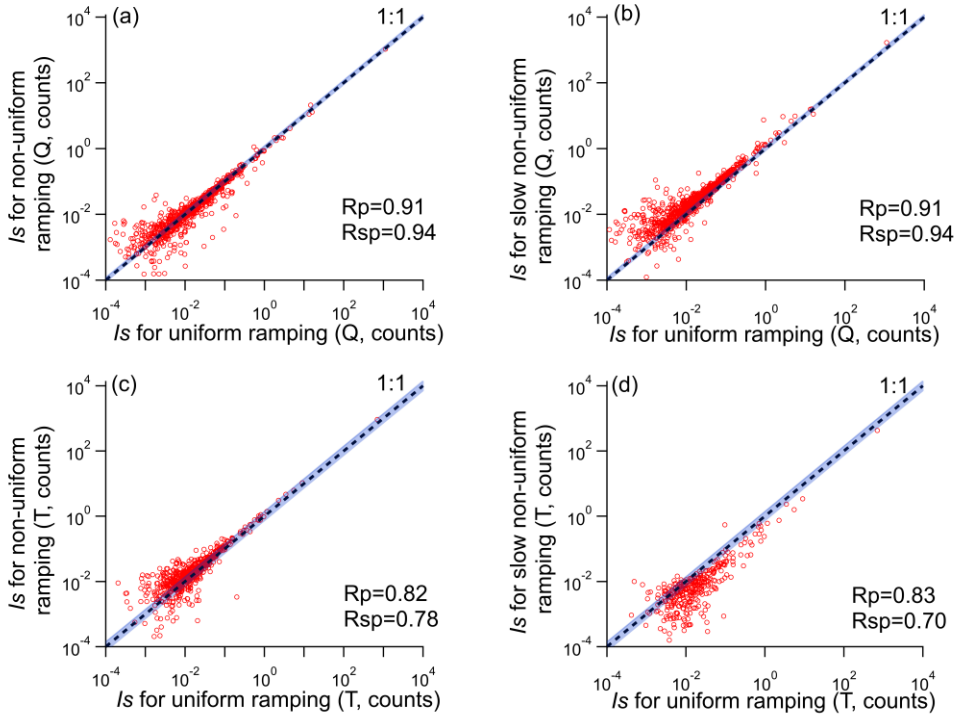

Figure 5. Comparison of *Is* from the different temperature ramping protocols of the 24-h Quartz (Q) and Teflon (T) filter samples, (a) non-uniform and uniform ramping (Quartz sample), (b) slow non-uniform and uniform ramping (Quartz sample), (c) non-uniform and uniform ramping (Teflon sample), (d) slow non-uniform and uniform ramping (Teflon sample). The blue shaded areas represent the relative error of signal assessed in the reproducibility tests of the 24-h samples (18% for Teflon and 9% for Quartz filters). The upper and lower limits for the reproducibility-based variation are calculated as (1+18%)/(1-18%) and (1-18%)/(1+18%), respectively. The upper and lower limits for the *Is* distribution of Quartz caused by reproducibility are calculated as (1+9%)/(1-9%) and (1-9%)/(1+9%), respectively.

For further analyses, we use the results from the non-uniform temperature ramping protocol, which represents a good balance between the influence of background due to low signal-to-noise ratios, and I^- depletion. The good agreement between offline FIGAERO-CIMS and ToF-ACSM discussed in Section 3.5 further implies that such a ramping protocol is suitable for the OA loadings observed in our study.

3.4 Linearity of signal response

To assess the linearity of signal response to the amount of sample collected on the filter, we used punches with varying areas from one single filter. We used punch diameters of 2, 3, 4, and 7 mm for a Teflon filter and 2 mm and 3 mm for a Quartz filter. The analytical protocol was kept constant between the individual sample punches (non-uniform ramping protocol and method 2b for background subtraction). The mass loadings of the analyzed filter punches ranged from 1.2 to 15 μg OA (2.2 to 27 μg $PM_{2.5}$) for the Teflon filter and from 1.2 to 2.7 μg OA (2.2 to 5.0 μg $PM_{2.5}$) for the Quartz filter (Table 1). The blank-subtracted *Is* from the different punching areas for the Quartz and Teflon filters is shown in Fig. 6. Overall, the offline FIGAERO-CIMS approach responds linearly to changes in filter mass loadings. The integrated signal ratios of CHOX are consistent with their respective area ratios (Figs. 6a, 6b), within uncertainty. In Fig. 6c we also plot the signal ratios of the 2 mm punch to the other punches, normalized by punching area (where 1 signifies perfect linearity). These ratios are generally in the range of possible variability caused by the relative error from the reproducibility tests.

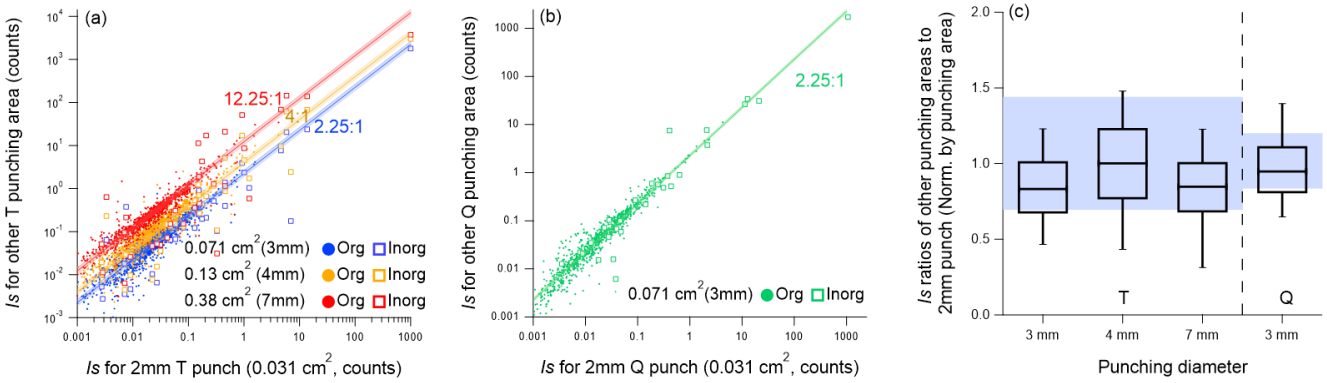

Figure 6. Comparison of the *Is* between signals from punches (a) with 3 mm, 4 mm, 7 mm, and 2 mm in diameter for the same Teflon filter, and (b) with 3mm and 2 mm in diameter for the same Quartz filter. The lines in (a) and (b) represent the punching area ratios. The shaded areas in (a) and (b) represent the area ratio plus/minus the relative errors (9% for Quartz, and 18% for Teflon) from the reproducibility tests. (c) Distribution of *Is* ratios normalized by the punching area ratios (3 mm, 4 mm, and 7 mm to 2 mm diameter punches for Teflon, 3 mm to 2 mm diameter punches for Quartz). Within each box, the median (middle horizontal line), 25^{th} and 75^{th} percentiles (lower and upper ends of the box), and 10^{th} and 90^{th} percentiles (lower and upper whiskers) are shown. The shaded area in (c) represents the possible distribution of the *Is* ratios due to the relative error established from the 24-h sample reproducibility tests (18% for Teflon and 9% for Quartz filters). The upper and lower limits for the Teflon *Is* ratio distribution are calculated as (1+18%)/(1-18%) and (1-18%)/(1+18%), respectively. The upper and lower limits for the Quartz *Is* ratio distribution are calculated as (1+9%)/(1-9%) and (1-9%)/(1+9%), respectively.

For compounds with very high signals, the response *Is* ratio can deviate from the punch area ratio, not least also due to the varying degree of reagent ion depletion. The highest I^- depletions were ~35%, ~60%, ~68%, and ~70% for 2mm, 3mm, 4mm, and 7mm punches, respectively. For e.g. the highest inorganic (HNO_3I^-) and organic ($C_6H_{10}O_5I^-$) ions, the *Is* from a 7mm punch is only 30% and 67%, respectively, of what would be expected based on punching area ratios (7mm to 2mm). For smaller punches (4 mm/3 mm), 75%/80% and 105%/107% of the expected HNO_3I^- and $C_6H_{10}O_5I^-$ signals, respectively, are detected. This indicates that for reduced amounts of desorbing material provided by smaller filter fractions, the amount of reagent ion is sufficient during the whole ramping process (lowest $I^-/C_6H_{10}O_5I^-$ signal ratio: ~10^3). In other words, if titration of reagent ion can be avoided as much as possible (e.g. I^-/target ion signal ratio: ~10^3) the *Is* responds linearly to concentration changes. In this study, titration is non-apparent for OA loadings of <5 μg and I^- signals of ~1 million. Therefore, it is recommended to calculate OA loadings of the samples prior analysis to determine the punching sizes in offline FIGAERO-CIMS analysis.

3.5 Comparison between offline FIGAERO-CIMS and *in-situ* ToF-ACSM

In the following, we compare the time series of the signals from offline FIGAERO-CIMS from Quartz filters and the corresponding chemical components from online ToF-ACSM measurement. The comparison between the total signal of all identified CHOX compounds and OA concentrations from the ToF-ACSM is displayed in Fig.7a. Here, the FIGAERO-CIMS signals of five polyols ($C_8H_{18}O_5I^-$, $C_{10}H_{22}O_6I^-$, $C_{12}H_{26}O_7I^-$, $C_{14}H_{30}O_8I^-$, $C_{16}H_{34}O_9I^-$) were excluded, which were contaminants from the lab due to their inexplicably high *Is* in 3 of the 27 12-h samples and the usage of diethylene glycol (DEG) in the lab. To compare with the $PM_{2.5}$ component concentrations from the ToF-ACSM, for each 12-h filter, we compute the sum of integrated signals (*Is*, signal integration over the entire thermogram, counts) multiplied by their molecular weight (MW, g mol^{-1}) of all compounds from FIGAERO-CIMS for comparison to the corresponding $PM_{2.5}$ component concentrations from the ToF-ACSM. Even though I^- is selective towards oxygenated organic compounds, the total MW-weighted CHOX signal measured by offline FIGAERO-CIMS in this study highly correlates with OA measured by the ToF-ACSM (Rp = 0.94), which is known to be dominated by secondary organic aerosols (SOA) (Cai et al., 2020; Kulmala et al., 2021; Jia et al., 2008).

The time series of the 12h-*Is* for HNO_3I^- and SO_3I^- measured by offline FIGAERO-CIMS correlate well with the NO_3 and SO_4 concentrations from ToF-ACSM (Rp = 0.94 and 0.95, Fig. 7b). The signal of HNO_3I^- in the particle phase measured by FIGAERO-CIMS is as an indicator of particulate nitrate and organonitrate (Lee et al., 2016), and the signal of SO_3I^- is related to inorganic sulfate and sulfur-containing organics (Ye et al., 2021; Cao et al., 2019). Following the same method, after calibrations, the quantified CHOX mass concentrations of offline FIGAERO-CIMS were found to be highly correlated with OA and SOA from ToF-ACSM in another dataset at the Peking University campus (PKU) in Beijing, indicating offline FIGAERO-CIMS analysis can be quantitative with proper calibrations (shown in Fig. S12 (Zheng et al., 2021)). Like other offline sampling methods, the offline FIGAERO-CIMS method may be affected by artefacts from sampling and storage of the filters. Both positive (absorption of gaseous OA), and negative artefacts (volatilization of collected OA), may occur during the sampling and storage, even if filters were stored frozen (Cheng et al., 2009). However, the signals from FIGAERO-CIMS correlate generally well with major components measured by TOF-ACSM, suggesting that those artefacts can be considered minor in our study, at least in terms of bulk PM constituents (Figure 7).

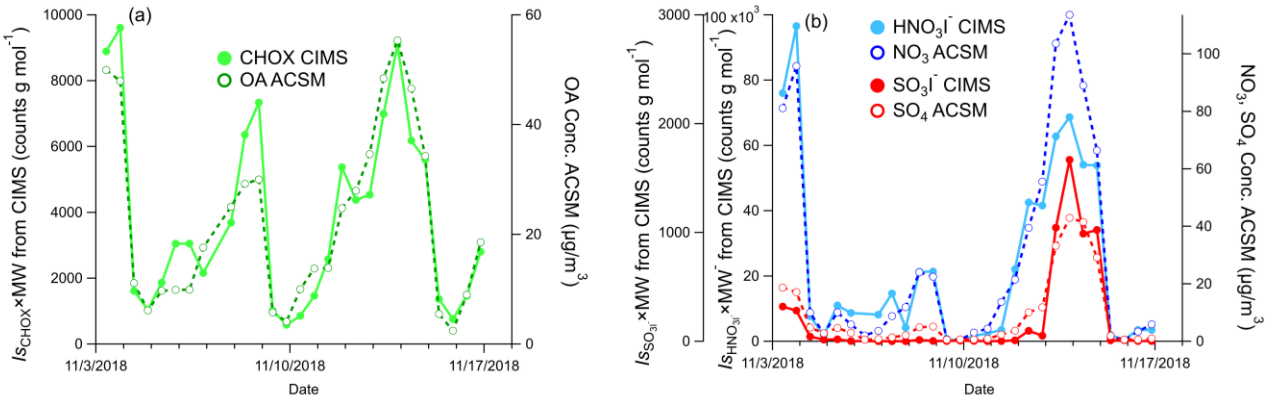

Figure 7. Comparison of the time series of the integrated signals of inorganic and organic compounds from 12-h samples (2 mm punches) analyzed by offline FIGAERO-CIMS, and chemical components measured in-situ by ToF-ACSM, (a) total CHOX from FIGAERO-CIMS and OA from ToF-ACSM, (b) HNO_3I^- from FIGAERO-CIMS and NO_3 from ToF-ACSM, (c) SO_3I^- from FIGAERO-CIMS and SO_4 from ToF-ACSM. To compare with the $PM_{2.5}$ component concentrations from the ToF-ACSM, the *Is* of each compound from FIGAERO-CIMS was multiplied by their molecular weight (MW) in (a) and (b). Note that FIGAERO-CIMS and ToF-ACSM data are on different axes

3.6 Comparison of Quartz and Teflon filters

In the following, we compare the *Is* from simultaneously collected Quartz and Teflon filter samples (collection times 2.5 h, 12 h, and 24 h, see Table 1). Fig. 8a and b show the comparison of the average *Is* of compounds (3 samples each) for both filter types, with 2.5h (OA loading of 9.1×10^{-2} µg) and 24h (OA loading of 1.2 µg) collection times. The mass spectra show an overall similar pattern, we observe a non-negligible difference, especially for the 2.5h samples (Fig. 8a). The log-transformed signals from Quartz and Teflon samples correlate better for 24-h samples (Rp = 0.96, Rsp = 0.95, Fig. S11d) than for the 2.5-h samples (Rp = 0.88, Rsp = 0.87, Fig. S11c). In addition, the signal observed for Quartz filter samples is generally slightly lower than for Teflon filter samples (Fig. 8c, d). Compounds with high Quartz/Teflon-signal ratios are in general semi- or low volatile compounds (operationally defined as having a T_{max}<60 °C). These compounds tend to be in the CHO and especially CHON category and exhibit a higher degree of unsaturation (e.g. $C_8H_6O_3I^-$, $C_6H_5NO_3I^-$ and $C_7H_6NO_3I^-$). They can be aromatics or their thermal fragmentation products (Liu et al., 2019). Due to the high surface area of the Quartz filters, semi- or low volatile compounds are more easily adsorbed than on Teflon filters, potentially resulting in higher positive artefacts. Compounds with low Quartz/Teflon-signal ratios tend to have overall low signal. Despite the application of a blank determination method that takes instrument backgrounds into account (Method 2b), higher residuals were still observed for the lower signal compounds, especially for the Teflon filters (as seen also for the 2.5-h and 0.5-h sample comparison (Fig. 3d). In contrast, compounds with a higher signal tend to be in the range of Q/T ratios expected based on the observed variability from the reproducibility tests (shown in Fig. 8c and 8d).

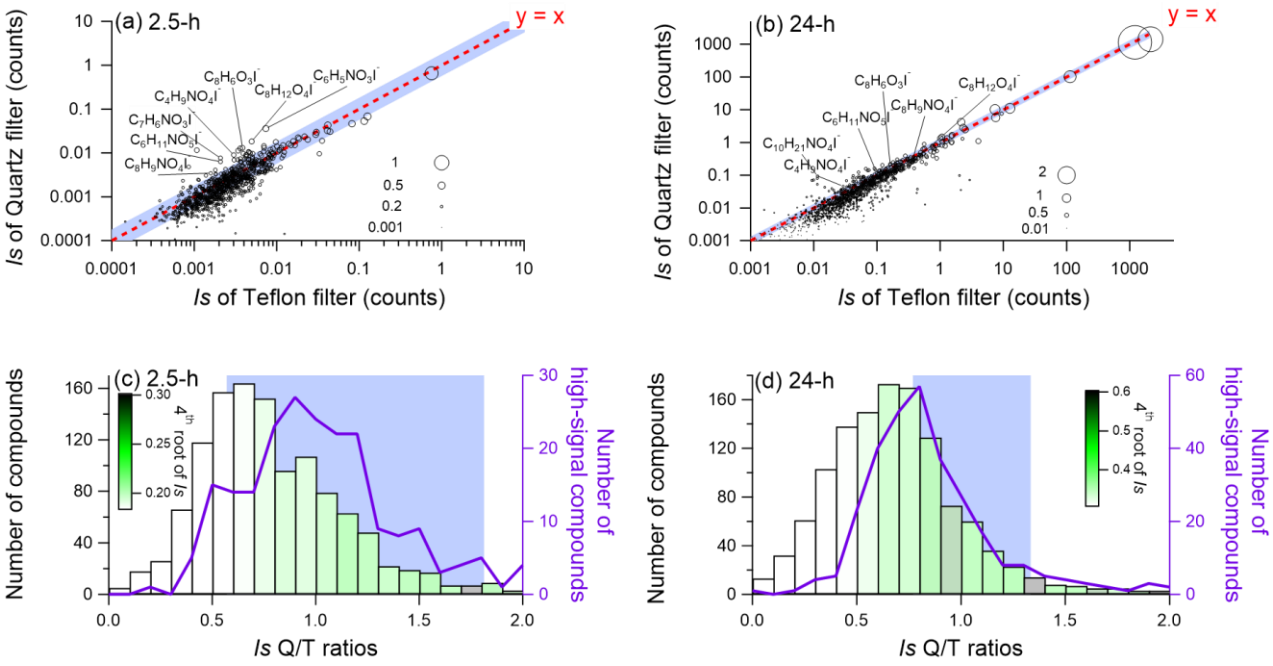

Figure 8. Comparison of the integrated signal intensities of all identified compounds for the Quartz fiber and Teflon filter samples for (a) 2.5-h samples, and (b) 24-h samples. The size of symbols in (a) and (b) is proportional to the 4th root of the signal intensity of each compound from the Quartz filter. Frequency distribution (number of compounds) per signal ratio of Quartz/Teflon for all compounds (green bars), and high-signal compounds (highest 25% signal compounds) only (purple lines) for 2.5-h samples (c), and 24-h samples (d). The bars in (c) and (d) are colored by the average of the 4th root of the signal intensity of the Quartz filter. The blue shaded area in each panel represents the possible distribution of *Is* ratios of Quartz/Teflon from the relative errors from the duplicate tests of 2.5-h (25% for Quartz and 31% for Teflon) and 24-h (9% for Quartz and 18% for Teflon) samples. The upper and lower limits for the 2.5-h Quartz/Teflon *Is* ratios were calculated as (1+25%)/(1-31%) and (1-25%)/(1+31%), respectively. The upper and lower limits for the 24-h Quartz/Teflon Is ratios were calculated as (1+9%)/(1-18%) and (1-9%)/(1+18%), respectively.

3.7 T_{max}: Influence of temperature ramping protocol and filter type

Non-uniform ramping of the temperature due to reagent ion titration is more likely needed when the FIGAERO-CIMS is run in offline mode compared to online mode, where sampling times and resulting filter mass loadings can be adjusted more easily. We have therefore developed a method (see section 2.2.4) to recover T_{max} from non-uniform ramping protocols, i.e. to make it comparable to T_{max} from uniform ramping protocols. Compared to the raw thermograms, the shape of the corrected thermograms is more similar to that of the uniform protocol (Fig. S13 and S14), since the thermograms were re-gridded to the same temperature intervals (3 °C).

Firstly, we tested the variation of T_{max} from the three duplicate tests of the Quartz filters using the non-uniform ramping protocol and thermogram correction (Fig. 9a). After correction, the corrected T_{max} ($T_{max\_nonuni\_corr}$) from individual tests was highly correlated with their average ($T_{max\_corr\_avg}$, Rp = 0.87–0.93). The median value of the difference between $T_{max\_nonuni\_corr}$ of duplicate tests and their average for all compounds ranges from -2.7–0.7 °C (shown in Fig.9b). The majority of compounds (52%–70%) have a T_{max} difference within 5 °C, close to the value reported in previously (~2°C, (Lopez-Hilfiker et al., 2014)). The median standard deviation of the difference between the corrected T_{max} of individual tests ($T_{max\_nonuni\_corr}$) and their average ($T_{max\_corr\_avg}$) from all compounds is 5.7 °C, which is defined as the variation of T_{max} for duplicate tests.

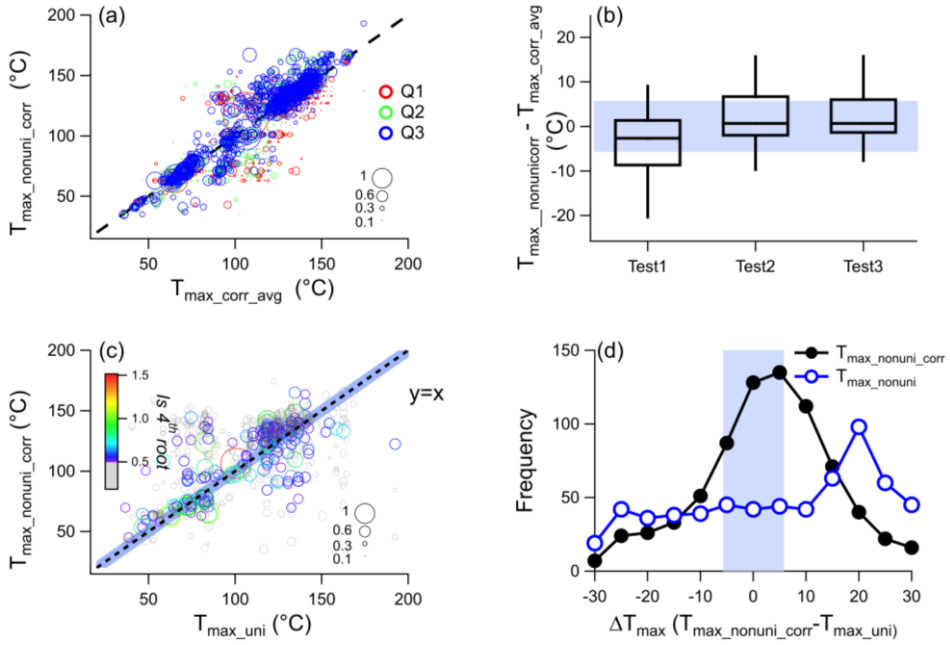

Figure 9. (a) Comparison of $T_{max\_nonuni\_corr}$ from the 3 duplicate tests and their average ($T_{max\_corr\_avg}$), (b) distribution of the difference between the 3 triplicate tests and the $T_{max\_corr\_avg}$, (c) comparison of T_{max} from the corrected non-uniform ramping and uniform ramping protocol (T_{max_uni}), (d) histogram of ΔT_{max} between T_{max} from the uniform ramping protocol (T_{max_uni}) and non-uniform with ($T_{max\_nonuni\_corr}$)/without (T_{max_nonuni}) correction. The size of symbols in (a) and (b) is proportional to the 4th root of the integrated signal intensity. The 4th root of the signal intensity <0.5 is shown in grey. The uniform ramping protocol test and 3 duplicate non-uniform ramping protocol tests were conducted for the same 24-h Quartz filter (Nov 23 to 24). The shaded area in (b), (c), and (d) represents T_{max} variation (±5.7°C) from the duplicate tests.

We take the uniform sampling protocol (see Fig. 1d) as the basis since this is the commonly used protocol for FIGAERO-CIMS in online mode. The comparison of T_{max} from the corrected non-uniform and the uniform ramping protocols is shown in Fig. 9c. Generally, after correction for the non-uniform ramping, the Pearson correlation coefficient of $T_{max\_nonuni\_corr}$ and T_{max_uni} is higher (Rp = 0.60) compared to the uncorrected ones with the uniform protocol (Rp = 0.20, T_{max_nonuni} *vs* T_{max_uni}). The correlation coefficients were even higher (0.72 and 0.84) for the 400 and 100 compounds with the highest signal intensity. In Fig. 9d we plot the frequency distribution

of the differences between the corrected T_{max} ($T_{max\_nonuni\_corr}$) and T_{max} from the uniform protocol (T_{max_uni}) for each CHOX compound in the spectrum. For 73% of the compounds, the difference in T_{max} between the two ramping protocols lies between -15 and 15 °C, and 41 % of compounds exhibit a difference of 0 – ±5 °C.

In the next step, we compared the volatility derived from T_{max} for Quartz fiber and Teflon filters. We selected a number of inorganic and organic compounds, based on their high average signals for the whole sampling period, for comparison of thermograms from 12-h and 24-h Teflon and Quartz filters sampled in parallel (Table S1, Fig. 10). Compounds include HNO_3I^-, CHON ($C_6H_5NO_3I^-$, $C_7H_7NO_3I^-$) and CHOS ($CH_4SO_3I^-$, $C_2H_4SO_4I^-$) compounds as well as CHO compounds with $C_{num}\geq3$ ($C_3H_4O_4I^-$, $C_4H_6O_4I^-$, $C_5H_8O_4I^-$, $C_6H_8O_4I^-$, $C_6H_{10}O_4I^-$, $C_6H_{10}O_5I^-$). Compounds with $C_{num}<3$ (e.g. $CH_2O_2I^-$) were excluded due to possible gas-phase interference and more likely influenced by thermal decomposition. Some compounds exhibited similar thermogram shapes for the two types of filters, such as $C_6H_{10}O_5I^-$ and $CH_4SO_3I^-$, while for some other species, the thermograms were different. Taking $C_3H_4O_4I^-$ as an example, a bimodal thermogram shape with peaks around 100 °C and 150 °C was observed for the Quartz filter, while only a unimodal peak around 90 °C was observed for the Teflon filter. The different thermogram shapes of individual compounds for the different filter types might warrant further investigation with a focus on the role of filter type properties (such as pore size, thickness, absorption, and hydrophobic/hydrophilic properties).

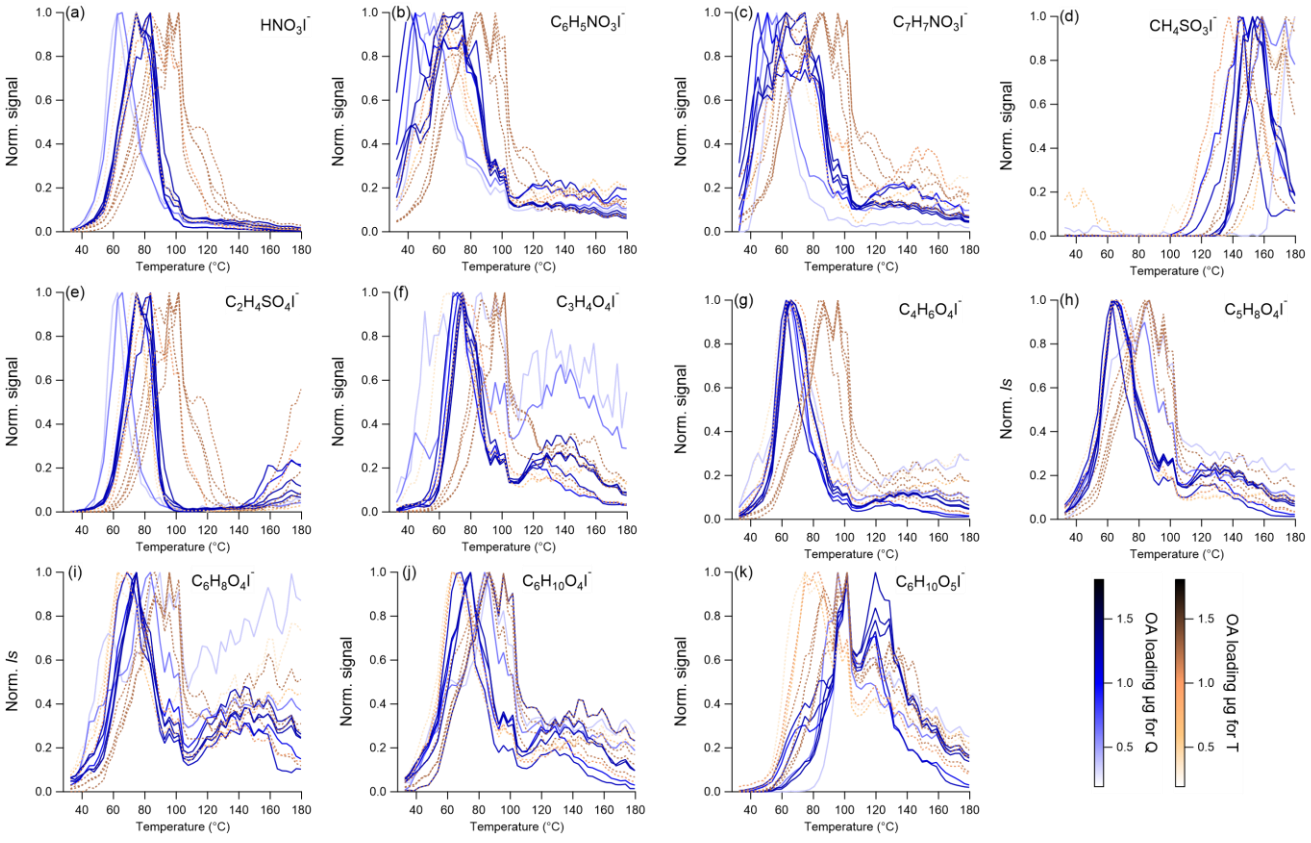

Figure 10. Normalized thermograms for Teflon (T, dashed lines) and Quartz (Q, solid lines) filters of, (a) HNO_3I^-, (b) $C_6H_5NO_3I^-$, (c) $C_7H_7NO_3I^-$, (d) $CH_4SO_3I^-$, (e) $C_2H_4SO_4I^-$, (f) $C_3H_4O_4I^-$, (g) $C_4H_6O_4I^-$, (h) $C_5H_8O_4I^-$, (i) $C_6H_8O_4I^-$, (j) $C_6H_{10}O_4I^-$, (k) $C_6H_{10}O_5I^-$. The thermograms were first corrected (section 2.2.4) and then normalized to signals in T_{max} and colored by the OA mass loading. The sampling information of the thermograms presented here is listed in Table S1.

In addition, we found that compounds with higher mass loadings appeared to have a higher T_{max} (e.g. $C_2H_4SO_4I^-$ and $C_7H_7NO_3I^-$, shown in Fig 10), consistent with previous findings using Teflon filters (Huang et al., 2018; Ylisirniö et al., 2021). The variability in T_{max} induced by varying PM loadings is within 5°C for 29% of compounds, and within 15°C for 54% of all compounds for Quartz filters, and 35% and 57% of compounds, respectively, for Teflon samples. The higher T_{max} variation for different OA loading samples compared to the duplicate samples (±5.7°C, Fig.9 b) is likely caused by other factors, such as particle viscosity, the particles on the filter, and/or mass loadings on the filter (Huang et al., 2018; Ylisirniö et al., 2021; Wu et al., 2021; Graham et al., 2022). The T_{max} variation due to filter type (Rp=0.27) is much larger than the one induced by filter loadings. Thus, the direct comparison of T_{max} between Quartz and Teflon filters is not feasible, warranting further research.

4. Discussion

This study introduces methods and assesses the performance of using the FIGAERO-CIMS in offline mode, i.e. to analyze particulate matter collected temporally and locally distant from the instrument on filter samples (Quartz and Teflon). Such an approach greatly enhances the capabilities of the FIGAERO-CIMS for analyzing atmospheric samples, as it enables the probing of the air at locations where and on occasions when *in-situ* deployments are difficult.

Due to the difficulties in background determination for offline FIGAERO-CIMS, in this study, we propose different background determination methods, which were further assessed by the comparison between samples from 5 different 0.5-h samples and a 2.5-h sample collected in parallel. We applied non-uniform temperature ramping to avoid reagent ion titration and a background scaling method taking interference of variable instrument backgrounds into account. In general, the offline FIGAERO-CIMS approach using the methods presented in this study can be used for providing OA composition information with typical offline sampling times (e.g. 12h and 24h) samples: (1) the reproducibility of integrated signal intensity is within ±20% for both filter types (18% for Teflon and 9% for Quartz), (2) detected signals respond linearly to changes in the samples' mass loadings, (3) the signals of CHOX and SO_3I^-, HNO_3I^- correlated well with corresponding $PM_{2.5}$ chemical component concentrations of OA, SO_4, and NO_3 measured by ToF-ACSM (Rp= 0.94 to 0.95), (4) the log-transformed mass spectra are highly correlated (Rp>0.9) between Quartz and Teflon filters for typical offline sampling times (e.g. 12h and 24h), and for high-signal compounds the *Is* ratios between Quartz and Teflon filters are generally within reproducibility variation. Overall, this highlights the possibility of using widely available and stored Quartz filters to identify CHOX molecular composition with FIGAERO-CIMS.

T_{max} retrieved from corrected thermograms of desorption with non-uniform ramping protocols are comparable to T_{max} from uniform ramping protocol for high signal intensity compounds (Rp = 0.72–0.84). More than 50% of compounds have T_{max} values that are reproducible within 5 °C for duplicate tests (Rp = 0.87–0.93) of the same sample, and for >50% of compounds, T_{max} varies within 15 °C for different mass loadings. Yet, T_{max} is strongly affected by the filter material (Teflon *vs* Quartz) leading to a large discrepancy in T_{max} between Quartz and Teflon samples (Rp = 0.27), hindering direct comparisons and warranting further research.

In summary, using FIGAERO-CIMS to analyze offline samples is a useful and simple way to investigate OA molecular composition, but care needs to be taken for T_{max} analyses. This opens broad applications to study OA molecular composition, sources, and formation processes at several sites simultaneously and in long-term deployments.

Author contributions

JC, KRD, CM, and MK designed the research. JC, FXZ, and WD collected the samples at the BUCT site. JC, CW, SH, KRD, and CM analyzed the samples and interpreted the data. ZY and CQ analyzed the samples collected at

the Peking University campus site. CM, KRD, and MK supervised this research. JC, KRD, and CM wrote the manuscript with contributions from all co-authors. All authors have given approval to the final version of this manuscript.

Acknowledgements

The work is supported by the Knut and Alice Wallenberg Foundation (WAF project CLOUDFORM, grant no. 2017.0165), the Academy of Finland (Center of Excellence in Atmospheric Sciences, project no. 307331, and PROFI3 funding, 311932, ACCC Flagship 337549), the European Research Council via ATM-GTP (742206), Wihuri Foundation, and the Jane and Aatos Erkko Foundation. KRD acknowledges support by the SNF mobility grant P2EZP2_181599. The authors also would like to thank Federico Bianchi's kind help and suggestions as well as the effort from all the researchers in the BUCT project to maintain the BUCT site.

Reference

Bannan, T. J., Le Breton, M., Priestley, M., Worrall, S. D., Bacak, A., Marsden, N. A., Merha, A., Hammes, J., Hallquist, M., Alfarra, M. R., Krieger, U. K., Reid, J. P., Jayne, J., Robinson, W., McFiggans, G., Coe, H., Percival, C. J., and Topping, D.: A method for extracting calibrated volatility information from the FIGAERO-HR-ToF-CIMS and its application to chamber and field studies, Atmospheric Measurement Techniques Discussions, 1-12, 10.5194/amt-2018-255, 2018.

Cai, J., Zheng, M., Yan, C., Fu, H.-Y., Zhang, Y.-J., Li, M., Zhou, Z., and Zhang, Y.-H.: Application and Progress of Single Particle Aerosol Time-of-Flight Mass Spectrometry in Fine Particulate Matter Research, Chinese Journal of Analytical Chemistry, 43, 765-774, 10.1016/S1872-2040(15)60825-8, 2015.

Cai, J., Wu, C., Wang, J., Du, W., Zheng, F., Hakala, S., Fan, X., Chu, B., Yao, L., Feng, Z., Liu, Y., Sun, Y., Zheng, J., Yan, C., Bianchi, F., Kulmala, M., Mohr, C., and Daellenbach, K. R.: Influence of organic aerosol molecular composition on particle absorptive properties in autumn Beijing, Atmospheric Chemistry and Physics, 22, 1251-1269, 10.5194/acp-22-1251-2022, 2022.

Cai, J., Chu, B., Yao, L., Yan, C., Heikkinen, L. M., Zheng, F., Li, C., Fan, X., Zhang, S., Yang, D., Wang, Y., Kokkonen, T. V., Chan, T., Zhou, Y., Dada, L., Liu, Y., He, H., Paasonen, P., Kujansuu, J. T., Petäjä, T., Mohr, C., Kangasluoma, J., Bianchi, F., Sun, Y., Croteau, P. L., Worsnop, D. R., Kerminen, V.-M., Du, W., Kulmala, M., and Daellenbach, K. R.: Size-segregated particle number and mass concentrations from different emission sources in urban Beijing, Atmospheric Chemistry and Physics, 20, 12721-12740, 10.5194/acp-20-12721-2020, 2020.

Cao, L. M., Huang, X. F., Wang, C., Zhu, Q., and He, L. Y.: Characterization of submicron aerosol volatility in the regional atmosphere in Southern China, Chemosphere, 236, 124383, 10.1016/j.chemosphere.2019.124383, 2019.

Cappa, C. D., Onasch, T. B., Massoli, P., Worsnop, D. R., Bates, T. S., Cross, E. S., Davidovits, P., Hakala, J., Hayden, K. L., Jobson, B. T., Kolesar, K. R., Lack, D. A., Lerner, B. M., Li, S.-M., Mellon, D., Nuaaman, I., Olfert, J. S., Petäjä, T., Quinn, P. K., Song, C., Subramanian, R., Williams, E. J., and Zaveri, R. A.: Radiative Absorption Enhancements Due to the Mixing State of Atmospheric Black Carbon, Science, 337, 1078-1081, 2012.

Cheng, Y., He, K. B., Duan, F. K., Zheng, M., Ma, Y. L., and Tan, J. H.: Measurement of semivolatile carbonaceous aerosols and its implications: a review, Environ Int, 35, 674-681, 10.1016/j.envint.2008.11.007, 2009.

Daellenbach, K. R., Uzu, G., Jiang, J., Cassagnes, L. E., Leni, Z., Vlachou, A., Stefenelli, G., Canonaco, F., Weber, S., Segers, A., Kuenen, J. J. P., Schaap, M., Favez, O., Albinet, A., Aksoyoglu, S., Dommen, J., Baltensperger, U., Geiser, M., El Haddad, I., Jaffrezo, J. L., and Prevot, A. S. H.: Sources of particulate-matter air pollution and its oxidative potential in Europe, Nature, 587, 414-419, 10.1038/s41586-020-2902-8, 2020.

Fan, X., Cai, J., Yan, C., Zhao, J., Guo, Y., Li, C., Dällenbach, K. R., Zheng, F., Lin, Z., Chu, B., Wang, Y., Dada, L., Zha, Q., Du, W., Kontkanen, J., Kurtén, T., Iyer, S., Kujansuu, J. T., Petäjä, T., Worsnop, D. R., Kerminen, V.-M., Liu, Y., Bianchi, F., Tham, Y. J., Yao, L., and Kulmala, M.: Atmospheric gaseous hydrochloric and hydrobromic acid in urban Beijing, China: detection, source identification and potential atmospheric impacts, Atmospheric Chemistry and Physics, 21, 11437-11452, 10.5194/acp-21-11437-2021, 2021.
Farmer, D. K., Vance, M. E., Abbatt, J. P. D., Abeleira, A., Alves, M. R., Arata, C., Boedicker, E., Bourne, S., Cardoso-Saldana, F., Corsi, R., DeCarlo, P. F., Goldstein, A. H., Grassian, V. H., Hildebrandt Ruiz, L., Jimenez, J. L., Kahan, T. F., Katz, E. F., Mattila, J. M., Nazaroff, W. W., Novoselac, A., O'Brien, R. E., Or, V. W., Patel, S., Sankhyan, S., Stevens, P. S., Tian, Y., Wade, M., Wang, C., Zhou, S., and Zhou, Y.: Overview of HOMEChem: House Observations of Microbial and Environmental Chemistry, Environ Sci Process Impacts, 21, 1280-1300, 10.1039/c9em00228f, 2019.
Graham, E. L., Wu, C., Bell, D. M., Bertrand, A., Haslett, S. L., Baltensperger, U., El Haddad, I., Krejci, R., Riipinen, I., and Mohr, C., 10.5194/egusphere-2022-1043, 2022.
Guo, Y., Yan, C., Li, C., Ma, W., Feng, Z., Zhou, Y., Lin, Z., Dada, L., Stolzenburg, D., Yin, R., Kontkanen, J., Daellenbach, K. R., Kangasluoma, J., Yao, L., Chu, B., Wang, Y., Cai, R., Bianchi, F., Liu, Y., and Kulmala, M.: Formation of nighttime sulfuric acid from the ozonolysis of alkenes in Beijing, Atmospheric Chemistry and Physics, 21, 5499-5511, 10.5194/acp-21-5499-2021, 2021.
Gustafson, K. E. and Dickhut, R. M.: Particle/Gas Concentrations and Distributions of PAHs in the Atmosphere of Southern Chesapeake Bay, Environmental Science & Technology, 31, 140-147, 10.1021/es9602197, 1997.
Huang, R. J., Zhang, Y., Bozzetti, C., Ho, K. F., Cao, J. J., Han, Y., Daellenbach, K. R., Slowik, J. G., Platt, S. M., Canonaco, F., Zotter, P., Wolf, R., Pieber, S. M., Bruns, E. A., Crippa, M., Ciarelli, G., Piazzalunga, A., Schwikowski, M., Abbaszade, G., Schnelle-Kreis, J., Zimmermann, R., An, Z., Szidat, S., Baltensperger, U., El Haddad, I., and Prevot, A. S.: High secondary aerosol contribution to particulate pollution during haze events in China, Nature, 514, 218-222, 10.1038/nature13774, 2014.
Huang, W., Saathoff, H., Shen, X., Ramisetty, R., Leisner, T., and Mohr, C.: Chemical Characterization of Highly Functionalized Organonitrates Contributing to Night-Time Organic Aerosol Mass Loadings and Particle Growth, Environ Sci Technol, 53, 1165-1174, 10.1021/acs.est.8b05826, 2019a.
Huang, W., Saathoff, H., Shen, X., Ramisetty, R., Leisner, T., and Mohr, C.: Seasonal characteristics of organic aerosol chemical composition and volatility in Stuttgart, Germany, Atmospheric Chemistry and Physics, 19, 11687-11700, 10.5194/acp-19-11687-2019, 2019b.
Huang, W., Saathoff, H., Pajunoja, A., Shen, X., Naumann, K.-H., Wagner, R., Virtanen, A., Leisner, T., and Mohr, C.: <i>α</i>-Pinene secondary organic aerosol at low temperature: chemical composition and implications for particle viscosity, Atmospheric Chemistry and Physics, 18, 2883-2898, 10.5194/acp-18-2883-2018, 2018.
Jia, Y., Rahn, K. A., He, K., Wen, T., and Wang, Y.: A novel technique for quantifying the regional component of urban aerosol solely from its sawtooth cycles, Journal of Geophysical Research, 113, 10.1029/2008jd010389, 2008.
Kontkanen, J., Deng, C., Fu, Y., Dada, L., Zhou, Y., Cai, J., Dällenbach, K. R., Hakala, S., Kokkonen, T. V., Lin, Z., Liu, Y., Wang, Y., Yan, C., Petäjä, T., Jiang, J., Kulmala, M., and Paasonen, P., 10.5194/acp-2020-215, 2020.
Koss, A. R., Sekimoto, K., Gilman, J. B., Selimovic, V., Coggon, M. M., Zarzana, K. J., Yuan, B., Lerner, B. M., Brown, S. S., Jimenez, J. L., Krechmer, J., Roberts, J. M., Warneke, C., Yokelson, R. J., and de Gouw, J.: Non-methane organic gas emissions from biomass burning: identification, quantification, and emission factors from PTR-ToF during the FIREX 2016 laboratory experiment, Atmospheric Chemistry and Physics, 18, 3299-3319, 10.5194/acp-18-3299-2018, 2018.
Kulmala, M., Dada, L., Daellenbach, K. R., Yan, C., Stolzenburg, D., Kontkanen, J., Ezhova, E., Hakala, S., Tuovinen, S., Kokkonen, T. V., Kurppa, M., Cai, R., Zhou, Y., Yin, R., Baalbaki, R., Chan, T., Chu, B., Deng, C., Fu, Y., Ge, M., He, H., Heikkinen, L., Junninen, H., Liu, Y., Lu, Y., Nie, W., Rusanen, A., Vakkari, V., Wang, Y., Yang, G., Yao, L., Zheng, J., Kujansuu, J., Kangasluoma, J., Petaja, T., Paasonen, P., Jarvi, L., Worsnop, D., Ding, A., Liu, Y., Wang, L., Jiang, J., Bianchi, F., and Kerminen, V. M.: Is reducing new particle formation a plausible solution to mitigate particulate air pollution in Beijing and other Chinese megacities?, Faraday Discuss, 226, 334-347, 10.1039/d0fd00078g, 2021.

Le Breton, M., Psichoudaki, M., Hallquist, M., Watne, Å. K., Lutz, A., and Hallquist, Å. M.: Application of a FIGAERO ToF CIMS for on-line characterization of real-world fresh and aged particle emissions from buses, Aerosol Science and Technology, 53, 244-259, 10.1080/02786826.2019.1566592, 2019.
Lee, B. H., Lopez-Hilfiker, F. D., amp, apos, Ambro, E. L., Zhou, P., Boy, M., Petäjä, T., Hao, L., Virtanen, A., and Thornton, J. A.: Semi-volatile and highly oxygenated gaseous and particulate organic compounds observed above a boreal forest canopy, Atmospheric Chemistry and Physics, 18, 11547-11562, 10.5194/acp-18-11547-2018, 2018.
Lee, B. H., Mohr, C., Lopez-Hilfiker, F. D., Lutz, A., Hallquist, M., Lee, L., Romer, P., Cohen, R. C., Iyer, S., Kurten, T., Hu, W., Day, D. A., Campuzano-Jost, P., Jimenez, J. L., Xu, L., Ng, N. L., Guo, H., Weber, R. J., Wild, R. J., Brown, S. S., Koss, A., de Gouw, J., Olson, K., Goldstein, A. H., Seco, R., Kim, S., McAvey, K., Shepson, P. B., Starn, T., Baumann, K., Edgerton, E. S., Liu, J., Shilling, J. E., Miller, D. O., Brune, W., Schobesberger, S., D'Ambro, E. L., and Thornton, J. A.: Highly functionalized organic nitrates in the southeast United States: Contribution to secondary organic aerosol and reactive nitrogen budgets, Proc Natl Acad Sci U S A, 113, 1516-1521, 10.1073/pnas.1508108113, 2016.
Liu, L., Rao, Z., Wang, Y., Arandiyan, H., Gong, J., Liang, M., and Guo, F.: Characteristics and Health Risk Assessment of Semi-Volatile Organic Contaminants in Rural Pond Water of Hebei Province, Int J Environ Res Public Health, 16, 10.3390/ijerph16224481, 2019.
Liu, Q., Baumgartner, J., Zhang, Y., and Schauer, J. J.: Source apportionment of Beijing air pollution during a severe winter haze event and associated pro-inflammatory responses in lung epithelial cells, Atmospheric Environment, 126, 28-35, https://doi.org/10.1016/j.atmosenv.2015.11.031, 2016.
Liu, Y., Zhang, Y., Lian, C., Yan, C., Feng, Z., Zheng, F., Fan, X., Chen, Y., Wang, W., Chu, B., Wang, Y., Cai, J., Du, W., Daellenbach, K. R., Kangasluoma, J., Bianchi, F., Kujansuu, J., Petäjä, T., Wang, X., Hu, B., Wang, Y., Ge, M., He, H., and Kulmala, M.: The promotion effect of nitrous acid on aerosol formation in wintertime in Beijing: the possible contribution of traffic-related emissions, Atmospheric Chemistry and Physics, 20, 13023-13040, 10.5194/acp-20-13023-2020, 2020.
Lopez-Hilfiker, F. D., Pospisilova, V., Huang, W., Kalberer, M., Mohr, C., Stefenelli, G., Thornton, J. A., Baltensperger, U., Prevot, A. S. H., and Slowik, J. G.: An extractive electrospray ionization time-of-flight mass spectrometer (EESI-TOF) for online measurement of atmospheric aerosol particles, Atmospheric Measurement Techniques, 12, 4867-4886, 10.5194/amt-12-4867-2019, 2019.
Lopez-Hilfiker, F. D., Mohr, C., Ehn, M., Rubach, F., Kleist, E., Wildt, J., Mentel, T. F., Lutz, A., Hallquist, M., Worsnop, D., and Thornton, J. A.: A novel method for online analysis of gas and particle composition: description and evaluation of a Filter Inlet for Gases and AEROsols (FIGAERO), Atmospheric Measurement Techniques, 7, 983-1001, 10.5194/amt-7-983-2014, 2014.
Lopez-Hilfiker, F. D., Mohr, C., D'Ambro, E. L., Lutz, A., Riedel, T. P., Gaston, C. J., Iyer, S., Zhang, Z., Gold, A., Surratt, J. D., Lee, B. H., Kurten, T., Hu, W. W., Jimenez, J., Hallquist, M., and Thornton, J. A.: Molecular Composition and Volatility of Organic Aerosol in the Southeastern U.S.: Implications for IEPOX Derived SOA, Environ Sci Technol, 50, 2200-2209, 10.1021/acs.est.5b04769, 2016.
Masoud, C. G., Li, Y., Wang, D. S., Katz, E. F., DeCarlo, P. F., Farmer, D. K., Vance, M. E., Shiraiwa, M., and Hildebrandt Ruiz, L.: Molecular composition and gas-particle partitioning of indoor cooking aerosol: Insights from a FIGAERO-CIMS and kinetic aerosol modeling, Aerosol Science and Technology, 56, 1156-1173, 10.1080/02786826.2022.2133593, 2022.
Mohr, C., Thornton, J. A., Heitto, A., Lopez-Hilfiker, F. D., Lutz, A., Riipinen, I., Hong, J., Donahue, N. M., Hallquist, M., Petaja, T., Kulmala, M., and Yli-Juuti, T.: Molecular identification of organic vapors driving atmospheric nanoparticle growth, Nat Commun, 10, 4442, 10.1038/s41467-019-12473-2, 2019.
Noziere, B., Kalberer, M., Claeys, M., Allan, J., D'Anna, B., Decesari, S., Finessi, E., Glasius, M., Grgic, I., Hamilton, J. F., Hoffmann, T., Iinuma, Y., Jaoui, M., Kahnt, A., Kampf, C. J., Kourtchev, I., Maenhaut, W., Marsden, N., Saarikoski, S., Schnelle-Kreis, J., Surratt, J. D., Szidat, S., Szmigielski, R., and Wisthaler, A.: The molecular identification of organic compounds in the atmosphere: state of the art and challenges, Chem Rev, 115, 3919-3983, 10.1021/cr5003485, 2015.

Riipinen, I., Yli-Juuti, T., Pierce, J. R., Petäjä, T., Worsnop, D. R., Kulmala, M., and Donahue, N. M.: The contribution of organics to atmospheric nanoparticle growth, Nature Geoscience, 5, 453-458, 10.1038/ngeo1499, 2012.
Schauer, J. J., Kleeman, M. J., Cass, G. R., and Simoneit, B. R. T.: Measurement of Emissions from Air Pollution Sources. 4. C1−C27 Organic Compounds from Cooking with Seed Oils, Environmental Science & Technology, 36, 567-575, 10.1021/es002053m, 2002.
Siegel, K., Zieger, P., Salter, M., Riipinen, I., Ekman, A. M. L., and Mohr, C.: Chemical composition of summertime High Arctic aerosols using chemical ionization mass spectrometry, May 01, 20202020.
Siegel, K., Karlsson, L., Zieger, P., Baccarini, A., Schmale, J., Lawler, M., Salter, M., Leck, C., Ekman, A. M. L., Riipinen, I., and Mohr, C.: Insights into the molecular composition of semi-volatile aerosols in the summertime central Arctic Ocean using FIGAERO-CIMS, Environmental Science: Atmospheres, 10.1039/d0ea00023j, 2021.
Tao, J., Zhang, L., Cao, J., and Zhang, R.: A review of current knowledge concerning PM_{2. 5} chemical composition, aerosol optical properties and their relationships across China, Atmospheric Chemistry and Physics, 17, 9485-9518, 10.5194/acp-17-9485-2017, 2017.
Thornton, J. A., Mohr, C., Schobesberger, S., D'Ambro, E. L., Lee, B. H., and Lopez-Hilfiker, F. D.: Evaluating Organic Aerosol Sources and Evolution with a Combined Molecular Composition and Volatility Framework Using the Filter Inlet for Gases and Aerosols (FIGAERO), Accounts of Chemical Research, 53, 1415-1426, 10.1021/acs.accounts.0c00259, 2020.
Turpin, B. J. and Lim, H.-J.: Species Contributions to PM2.5 Mass Concentrations: Revisiting Common Assumptions for Estimating Organic Mass, Aerosol Science and Technology, 35, 602-610, 10.1080/02786820119445, 2001.
Turpin, B. J., Saxena, P., and Andrews, E.: Measuring and simulating particulate organics in the atmosphere: problems and prospects, Atmospheric Environment, 34, 2983-3013, https://doi.org/10.1016/S1352-2310(99)00501-4, 2000.
Wang, J. M., Jeong, C.-H., Hilker, N., Shairsingh, K. K., Healy, R. M., Sofowote, U., Debosz, J., Su, Y., McGaughey, M., Doerksen, G., Munoz, T., White, L., Herod, D., and Evans, G. J.: Near-Road Air Pollutant Measurements: Accounting for Inter-Site Variability Using Emission Factors, Environmental Science & Technology, 52, 9495-9504, 10.1021/acs.est.8b01914, 2018.
Watson, J. G. and Chow, J. C.: Comparison and evaluation of in situ and filter carbon measurements at the Fresno Supersite, Journal of Geophysical Research: Atmospheres, 107, ICC 3-1-ICC 3-15, 10.1029/2001jd000573, 2002.
Wu, C., Bell, D. M., Graham, E. L., Haslett, S., Riipinen, I., Baltensperger, U., Bertrand, A., Giannoukos, S., Schoonbaert, J., El Haddad, I., Prevot, A. S. H., Huang, W., and Mohr, C.: Photolytically induced changes in composition and volatility of biogenic secondary organic aerosol from nitrate radical oxidation during night-to-day transition, Atmospheric Chemistry and Physics, 21, 14907-14925, 10.5194/acp-21-14907-2021, 2021.
Yao, L., Garmash, O., Bianchi, F., Zheng, J., Yan, C., Kontkanen, J., Junninen, H., Mazon, S. B., Ehn, M., Paasonen, P., Sipila, M., Wang, M. Y., Wang, X. K., Xiao, S., Chen, H. F., Lu, Y. Q., Zhang, B. W., Wang, D. F., Fu, Q. Y., Geng, F. H., Li, L., Wang, H. L., Qiao, L. P., Yang, X., Chen, J. M., Kerminen, V. M., Petaja, T., Worsnop, D. R., Kulmala, M., and Wang, L.: Atmospheric new particle formation from sulfuric acid and amines in a Chinese megacity, Science, 361, 278-+, 10.1126/science.aao4839, 2018.
Yao, L., Fan, X., Yan, C., Kurten, T., Daellenbach, K. R., Li, C., Wang, Y., Guo, Y., Dada, L., Rissanen, M. P., Cai, J., Tham, Y. J., Zha, Q., Zhang, S., Du, W., Yu, M., Zheng, F., Zhou, Y., Kontkanen, J., Chan, T., Shen, J., Kujansuu, J. T., Kangasluoma, J., Jiang, J., Wang, L., Worsnop, D. R., Petaja, T., Kerminen, V. M., Liu, Y., Chu, B., He, H., Kulmala, M., and Bianchi, F.: Unprecedented Ambient Sulfur Trioxide (SO3) Detection: Possible Formation Mechanism and Atmospheric Implications, Environ Sci Technol Lett, 7, 809-818, 10.1021/acs.estlett.0c00615, 2020.
Ye, C., Yuan, B., Lin, Y., Wang, Z., Hu, W., Li, T., Chen, W., Wu, C., Wang, C., Huang, S., Qi, J., Wang, B., Wang, C., Song, W., Wang, X., Zheng, E., Krechmer, J. E., Ye, P., Zhang, Z., Wang, X., Worsnop, D. R., and Shao, M.: Chemical characterization of oxygenated organic compounds in the gas phase and particle phase using iodide CIMS with FIGAERO in urban air, Atmos. Chem. Phys., 21, 8455-8478, 10.5194/acp-21-8455-2021, 2021.

Ylisirniö, A., Barreira, L. M. F., Pullinen, I., Buchholz, A., Jayne, J., Krechmer, J. E., Worsnop, D. R., Virtanen, A., and Schobesberger, S.: On the calibration of FIGAERO-ToF-CIMS: importance and impact of calibrant delivery for the particle-phase calibration, Atmos. Meas. Tech., 14, 355-367, 10.5194/amt-14-355-2021, 2021.
Zheng, Y., Chen, Q., Cheng, X., Mohr, C., Cai, J., Huang, W., Shrivastava, M., Ye, P., Fu, P., Shi, X., Ge, Y., Liao, K., Miao, R., Qiu, X., Koenig, T. K., and Chen, S.: Precursors and Pathways Leading to Enhanced Secondary Organic Aerosol Formation during Severe Haze Episodes, Environ Sci Technol, 55, 15680-15693, 10.1021/acs.est.1c04255, 2021.